

# Spin and thermal current scaling at a Y-junction of XX spin chains

Domenico Giuliano

*Dipartimento di Fisica, Università della Calabria Arcavacata di Rende I-87036, Cosenza, Italy and  
I.N.F.N., Gruppo collegato di Cosenza Arcavacata di Rende I-87036, Cosenza, Italy*

Francesco Bucchieri

*Dipartimento di Scienza Applicata e Tecnologia, Politecnico di Torino,  
Corso Duca degli Abruzzi 24, 10129, Torino, Italy and  
INFN Sezione di Torino, Via P. Giuria 1, I-10125, Torino, Italy*

We study the boundary phase diagram and the low-temperature heat and magnetization transport at a Y-junction of XX spin chains. Depending on the magnetization axis anisotropy between the magnetic exchange interactions at the junction, the system exhibits two different strong-coupling regimes at low energies/temperatures, similar to the overscreened (topological) four- and to the two-channel Kondo fixed points. Using renormalization group arguments combined with boundary conformal field theory methods, we show the instability of the former under any XY-type anisotropy at the junction. We analyze the low-temperature spin and the heat conductances. We find evidence of spin fractionalization of the elementary excitations at the four-channel Kondo fixed point by means of the magnetic Wiedemann-Franz law. We caution that the instability under XY anisotropy may hinder the detection of the phenomenology related to the four-channel Kondo effect, therefore requiring careful control in experimental realizations.

## I. INTRODUCTION

Energy flows in quantum systems are an important object of study in modern condensed matter physics: indeed, they lie at the heart of fundamental questions of out-of-equilibrium statistical physics. Of special interest for practical applications are one-dimensional models [1]. For example, driven spin chains can act as heat engines [2], which in theory allow for the conversion between energy and work at the quantum level [3, 4]. Anomalous heat conductance can be present in one dimension, in the presence of momentum-conserving lattices [5]. In addition, heat currents reflect the conservation laws of the systems at hand [6–8]. Many platforms support one-dimensional heat conduction channels. Realizations range from carbon nanotubes [9], atomic chains [10], metallic quantum wires, conventional and topological [11, 12], as well as one-dimensional edge channels in graphene [13].

In this study, we will be concerned, in particular, with spin chain materials and their cold-atomic emulators. The investigation of heat transport in magnetic systems has indeed elicited strong interest after the discovery of the spin-Seebeck effect [14], and established the whole field of spin caloritronics [15]. Remarkably, heat and magnetization currents have been demonstrated to be controllable at the microscopic level by magnetic fields and dissipation [16–18]. Even in purely spintronics applications, thermal management is an important aspect related to energy efficiency and performance [19]. Recent studies on caloric effects in spin chains suggest the potential of this class of systems to control heat fluxes at the quantum level [20, 21]. Such a control is also relevant for the new possibilities that atomic physics offers, in connection to the quantum technologies based on optically trapped ultracold atoms [22, 23]. Due to the

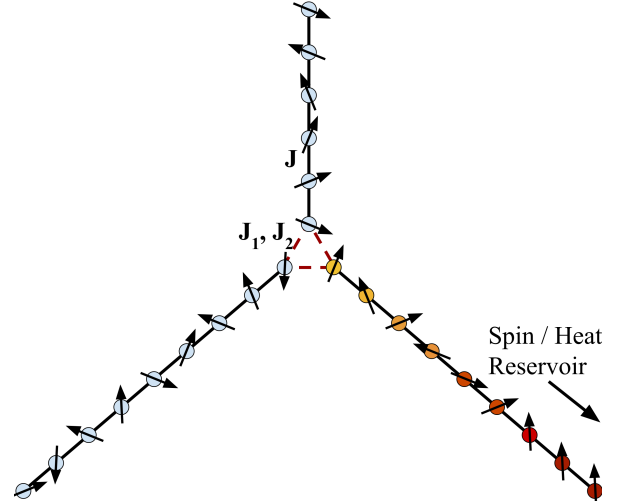


FIG. 1. Sketch of a Y junction of semi-infinite spin chains. The magnetic spin exchange interaction  $J$  along the three chains is the same along the  $x$ - and the  $y$ -directions and is represented by a black bond. In the central triangle the magnetic exchange interaction can be different in the different representation, which we represent by dashed red lines. Each chain is connected to a magnetization and temperature reservoir.

extremely low temperatures involved, all such platforms require careful and precise control of the energy flows within the system [24, 25].

In this work, we analyze in detail the simplest nontrivial magnetic circuit element, namely, the Y junction [26], see Fig. 1. The problem of heat transport in junctions and graphs has been tackled from a classical perspective [27, 28], as well as from a field-theoretical one [29–32]. The energy flows within the junction, arising from con-

tact with reservoirs at different temperatures, can be described in terms of non-equilibrium steady states [33, 34], in which the chiral low-energy excitations are in equilibrium with their sources. What motivates interest in spin chain junctions is that a variety of fixed points (FPs) are known, enabling control of magnetic excitation [35, 36], as well as the creation of highly entangled states [37, 38]. In presence of a gapless spectrum, a full Kondo cloud can indeed develop and modify the conduction properties of the FP [39–42]. This becomes manifest in a non-trivial thermal conductance, which remains nonetheless linear in temperature [32].

Insulating magnets can support ballistic magnonic heat and spin transport with universal behavior analogous to that of electrons [43, 44]. This is encoded in the magnonic Lorenz ratio

$$\mathcal{L}_m = \frac{\mathcal{J}_Q}{T \mathcal{J}_S}, \quad (1)$$

where  $\mathcal{J}_Q$  is the heat current,  $\mathcal{J}_S$  the spin current, and  $T$  the absolute temperature. In the low-temperature limit, the ratio asymptotically approaches a universal constant:

$\mathcal{L}_m = \frac{\pi^2}{3} \left( \frac{k_B}{g\mu_B} \right)^2$ , where  $g$  is the Landé  $g$ -factor and  $\mu_B$  is the Bohr magneton. This result is analogous to the Wiedemann-Franz law (WF) for electrons. In the magnonic case, the Lorenz ratio is independent of microscopic details such as the magnon dispersion or exchange coupling, and depends only on fundamental constants. This indicates a form of universality in magnon transport across insulating ferromagnetic junctions and provides theoretical foundation for designing spin conductors and energy-efficient spin caloritronic devices.

A key point in engineering efficient quantum devices is to make their behavior robust against fluctuations in microscopic system parameters, minor details on the system design, and so on. An effective way to achieve this goal is to work at an interacting renormalization group (RG) FP of its phase diagram. By means of a combined use of perturbative RG methods and conformal field theory techniques, several interacting FPs have been identified in the phase diagram of Y-junctions of quantum wires, spin chains and/or one-dimensional Josephson junction arrays. These exhibit several non-conventional properties, such as spin or charge fractionalization [26, 45–47], or pairing of Cooper pairs [48, 49]. Moreover, they can host nontrivial realizations of the multi-channel Kondo effect, including its topological version [31, 38–40, 50–55]. When aiming at realizing the nontrivial Kondo-like FP, it is essential to have control of the parameters at the junctions, due to the (marginal) relevance of some junction interaction. In general, the RG flow of the system toward a given attractive FP may strongly depend on the initial conditions on the system parameters. Nevertheless, it is known that fine tuning of the exchange interaction between different chain ends is unnecessary in the XX case, because the RG flow is robust against fluctuations at leading order [52, 56, 57]. However, the spin Y

junction contain another type of anisotropy, namely, exchange anisotropy, which can arise from purely geometric factors [58].

Motivated by the above observations, in this work, we characterize the FPs of a Y-junction of XX spin chains from the perspective of their RG flow. To map out the RG flow diagram and to characterize the various RG FPs, we make a combined use of perturbative RG methods combined with conformal field theory methods. Doing so, we derive the spin and the heat conductance tensor at the FPs, with emphasis on the magnonic equivalent of the WF [43]. In particular, after discussing in detail the physical properties of the various strongly interacting FPs of the system, we highlight the instability of the topological Kondo (TK) FP under XY interaction anisotropy at the junction, which prompts special care in tuning the microscopic parameters in experiments.

The paper is organized as follows: in Section II, we introduce the model Hamiltonian of our system, as well as the spin and heat currents. In Section III, we present the phase diagram of the junction. The following Sections contain the heat conductance and the discussion of the WF around the various FPs. In particular, in Section IV we lay out the perturbative approach around the disconnected FP, while in Section V and VI we respectively discuss the Ising and the TK FPs. We summarize our results in Section VII. Various Appendixes contain further details about the Keldysh formalism, the RG procedure and the effective theories at the FPs.

## II. MODEL OF THE JUNCTION

We sketch our system in Fig.1. The junction is made out of three XX chains connected to each other in a Y-shaped junction at one of their endpoints. The system Hamiltonian is therefore composed of a free chain term, which only describes the three chains,  $H_{XX3} = \sum_{\lambda=1}^3 H_{XX,\lambda}$ , with  $\lambda$  being the chain index, and of a boundary term  $H_K$ , describing the junction between the three chains. The relevant parameters entering each chains Hamiltonian are the exchange interaction strength  $J$  between nearest neighboring sites (that is planar in the spin space), and the applied magnetic field  $H$  (that lies along the  $z$  axis in spin space). As a result, the “bulk” Hamiltonian for a single chain is given by

$$H_{XX,\lambda} = -J \sum_{j=1}^{\ell-1} \{S_{j,\lambda}^x S_{j+1,\lambda}^x + S_{j,\lambda}^y S_{j+1,\lambda}^y\} + H \sum_{j=1}^{\ell} S_{j,\lambda}^z, \quad (2)$$

with  $J$  ( $> 0$ ) being the magnetic exchange coupling strength and  $H$  the applied Zeeman field. In Eq.(2) the quantum spin-1/2 operators  $S_{j,\lambda}^a$  obey the commutation relations  $[S_{j,\lambda}^a, S_{j',\lambda'}^b] = i \sum_c \epsilon^{a,b,c} \delta_{j,j'} \delta_{\lambda,\lambda'} S_{j,\lambda}^c$ , with  $\epsilon^{a,b,c}$  being the fully antisymmetric tensor. For simplicity,  $H$  is rescaled by the factor  $g\mu_B/\hbar$  and is therefore dimensionally a frequency. With this definition, the

Wiedemann-Franz law takes the form

$$\mathcal{L}_m = \frac{\pi^2}{3} \left( \frac{k_B}{\hbar} \right)^2 . \quad (3)$$

Also, we set the parameters of the three chains to be equal to each other, as the effect of fluctuations in these parameters are known to produce sub-leading corrections at the low-temperature fixed points [52, 56, 57].

As for the boundary Hamiltonian  $H_K$  describing the junction, in full generality we allow for an asymmetry between the  $x$ - and the  $y$ -axis in spin space, that is, we set:

$$H_K = -J_1 \sum_{\lambda=1}^3 S_{\lambda,1}^x S_{\lambda+1,1}^x - J_2 \sum_{\lambda=1}^3 S_{\lambda,1}^y S_{\lambda+1,1}^y , \quad (4)$$

with  $\lambda+3 \equiv \lambda$  understood when summing over the chain index. To study transport properties of our system, it is useful to trade it for a junction of lattice fermionic chains, possibly with a nontrivial boundary interaction term arising when describing the system in fermionic coordinates [36, 38, 39, 50, 51, 59, 60]. In order to do so, one has to extend the Jordan-Wigner (JW) transformation to a junction of three quantum spin chains by introducing three additional Klein factors,  $\{\eta_1, \eta_2, \eta_3\}$  [37], so that the transformations from spin to fermionic variables read

$$\begin{aligned} S_{j,\lambda}^+ &= i\eta_\lambda c_{\lambda,j}^\dagger e^{i\pi \sum_{r=1}^{j-1} c_{\lambda,r}^\dagger c_{\lambda,r}} \\ S_{j,\lambda}^- &= i\eta_\lambda c_{\lambda,j} e^{i\pi \sum_{r=1}^{j-1} c_{\lambda,r}^\dagger c_{\lambda,r}} \\ S_{j,\lambda}^z &= c_{\lambda,j}^\dagger c_{\lambda,j} - \frac{1}{2} , \end{aligned} \quad (5)$$

with  $S_{j,\lambda}^\pm = S_{j,\lambda}^x \pm iS_{j,\lambda}^y$ . The JW fermions satisfy canonical anticommutation relations

$$\{c_{j,\lambda}, c_{j',\lambda'}^\dagger\} = \delta_{j,j'} \delta_{\lambda,\lambda'} , \quad (6)$$

while the Klein factors satisfy the algebra

$$\{\eta_\lambda, \eta_{\lambda'}\} = 2\delta_{\lambda,\lambda'} , \quad (7)$$

Eqs.(6,7) imply that the canonical commutation relations for the quantum spin operators are naturally satisfied. When implementing Eqs.(5) the Klein factors disappear from the bulk Hamiltonian for the three chains. In JW fermionic coordinates we obtain

$$\begin{aligned} H_{XX,\lambda,f} &= \sum_{\lambda=1}^3 \left\{ -J \sum_{j=1}^{\ell-1} [c_{j,\lambda}^\dagger c_{j+1,\lambda} + c_{j+1,\lambda}^\dagger c_{j,\lambda}] \right. \\ &\quad \left. + H \sum_{j=1}^{\ell} c_{j,\lambda}^\dagger c_{j,\lambda} + \text{const} \right\} , \end{aligned} \quad (8)$$

with the over-all constant contribution being unimportant for the following calculations and, therefore, neglected henceforth. At variance, the Klein factors do appear in  $H_K$  which, in fermionic coordinates, reads

$$\begin{aligned} H_{K,f} &= \frac{1}{2} \sum_{\lambda=1}^3 \left\{ [-i\eta_\lambda \eta_{\lambda+1}] \times \right. \\ &\quad \left[ J_1 [-i(c_{\lambda,1}^\dagger + c_{\lambda,1})(c_{\lambda+1,1}^\dagger + c_{\lambda+1,1})] \right. \\ &\quad \left. \left. + J_2 [i(c_{\lambda,1}^\dagger - c_{\lambda,1})(c_{\lambda+1,1}^\dagger - c_{\lambda+1,1})] \right] \right\} . \end{aligned} \quad (9)$$

In the explicit expression for  $H_{K,f}$  in Eq.(9) we identify a Kondo-like interaction, with the “standard” Kondo impurity spin replaced by the “topological” spin operator  $\mathcal{T}_\lambda = -i\eta_{\lambda+1} \eta_{\lambda+2}$  (with  $\lambda+3 \equiv \lambda$ ) [39, 53, 57, 61]. The topological spin is coupled to two, independent spin operators made out of the lattice fermionic fields at the junction site,  $j = 1$ . As a result, one infers how the Kondo interaction Hamiltonian  $H_{K,f}$  corresponds to a doubled-channel version of the two-channel Kondo interaction, as proposed in [62], that is, to a topological, four-channel Kondo model [37, 56, 59].

As they are the key observable quantities we use throughout our paper to characterize the various FPs, we now derive the lattice formulas for the conserved spin- and heat-current operators. Let  $j$  and  $j+1$  denote sites in the bulk of a chain (that is, both different from 1 and  $\ell$ ), to site  $j$  we associate the spin density in the  $z$  direction given by  $S_{j,\lambda}^z = c_{j,\lambda}^\dagger c_{j,\lambda} - \frac{1}{2}$ . At the same time, to the link  $(j, j+1)$  we associate the energy density given by

$$\begin{aligned} \mathcal{E}_{(j,j+1),\lambda} &= -J \{ c_{j,\lambda}^\dagger c_{j+1,\lambda} + c_{j+1,\lambda}^\dagger c_{j,\lambda} \} \\ &\quad + \frac{H}{2} \{ c_{j,\lambda}^\dagger c_{j,\lambda} + c_{j+1,\lambda}^\dagger c_{j+1,\lambda} \} . \end{aligned} \quad (10)$$

If  $1 < j < \ell$ , the Heisenberg equation of motion for the operator  $c_{j,\lambda}(t)$  is given by

$$i\hbar \frac{\partial c_{j,\lambda}(t)}{\partial t} = -J \{ c_{j+1,\lambda}(t) + c_{j-1,\lambda}(t) \} + H c_{j,\lambda}(t) . \quad (11)$$

From Eqs.(11) we readily recover the continuity equations for the spin- and for the energy-density operators, that is

$$\frac{dS_{j,\lambda}^z}{dt} = -\{ \mathcal{J}_{S,j+1,\lambda} - \mathcal{J}_{S,j,\lambda} \} , \quad (12)$$

for the spin density, and

$$\frac{d\mathcal{E}_{(j,j+1),\lambda}}{dt} = -\{ \mathcal{J}_{Q,(j+1,1),\lambda} - \mathcal{J}_{Q,(j,j-1),\lambda} \} , \quad (13)$$

for the energy density, with

$$\begin{aligned} \mathcal{J}_{S,j,\lambda} &= -iJ \{ c_{j,\lambda}^\dagger c_{j+1,\lambda} - c_{j+1,\lambda}^\dagger c_{j,\lambda} \} \\ \mathcal{J}_{Q,(j+1,j),\lambda} &= i \frac{J^2}{\hbar} \{ c_{j,\lambda}^\dagger c_{j+2,\lambda} - c_{j+2,\lambda}^\dagger c_{j,\lambda} \} . \end{aligned} \quad (14)$$

We now derive the phase diagram of our system, a task for which we have to refer to the RG equations derived in Appendix B.

### III. PHASE DIAGRAM OF THE Y-JUNCTION OF XX CHAINS

The simplest FP in the phase diagram of our junction (the “disconnected FP, DFP”) corresponds to the full disconnection of the three chains from each other, that is, to  $J_1 = J_2 = 0$ . A nonzero  $J_1$  and/or  $J_2$  yield to nonperturbative effects which we account within RG approach in the corresponding running couplings. In Appendix A and B we present in detail the various steps leading to the RG equations. As a result, we find that, on lowering the high-energy cutoff from  $D$  to  $D - \delta D$ , the coupling strengths are renormalized according to the flow equations

$$\frac{dJ_{1,2}}{dD} = -\frac{6\varphi(D, H)}{\pi JD} J_{1,2}^2, \quad (15)$$

with

$$\varphi(D, H) = \left\{ 1 + \frac{D^2 - H^2}{2J^2} + \left[ \frac{D^2 + H^2}{4J^2} \right]^4 \right\}^{\frac{1}{4}} \times \cos \left[ \frac{1}{2} \operatorname{atan} \left( \frac{2HD}{4J^2 + D^2 - H^2} \right) \right]. \quad (16)$$

Eqs.(15) imply a growth of the running couplings on lowering the cutoff scale  $D$ . To second-order in the boundary couplings themselves, the equations decouple. The Kondo temperature pertinent to each channel,  $T_{K,(1,2)}$  can be computed by using the implicit equation

$$\frac{\pi J}{6J_{1,2}} = \int_{k_B T_{K,(1,2)}}^{D_0} \left[ \frac{\varphi(u, H)}{u} \right] du, \quad (17)$$

with  $D_0 \sim 2J$  (see Appendix B for details) which implies that, the higher temperature corresponds to the larger (“bare”) boundary coupling.

Let us, now, assume, for the sake of the following discussion, that  $J_1(D_0) > J_2(D_0)$ . Integrating Eqs.(15), we find that  $J_1(D)$  first crosses over to the strongly coupled regime at the corresponding Kondo scale  $D = D_{*,1} = k_B T_{K,1}$ . As we discuss in detail in Appendix C, at scales  $< D_{*,1}$  the junction flows towards the “Ising-like” FP  $\mathcal{I}_1$ , in which half of the real fermionic modes out of which the complex lead fermions are formed, conspire to screen the topological impurity spin, similarly with what happens at a Y junction of three Ising chains [39, 50, 51], while the other half contribute the over-all system dynamics only perturbatively in  $J_2$ . At variance, the complementary situation, in which  $J_2(D_0) > J_1(D_0)$ , implies a flow of the junction toward the complementary  $\mathcal{I}_2$  Ising-like FP.

Finally, as we discuss in Appendix D, when  $J_1(D_0) = J_2(D_0)$  the junction flows toward a FP analogous to the one corresponding to the strongly coupled regime of the TK model (TKM) [31, 52, 57]. At the TKM, the hybridization between the topological spin, determined

by the Klein factors, and the lead degrees of freedom yields a crossover in the boundary conditions of the “relative” bosonic fields  $\phi_\lambda(x) - \phi_{\lambda+1}(x)$  at  $x = 0$  from Neumann boundary conditions (corresponding to the DFP) to Dirichlet boundary conditions (corresponding to the strongly coupled TKM FP). Thus, on one hand we conclude that, as soon as one turns on nonzero  $J_1$  and/or  $J_2$ , the DFP is unstable, on the other hand, that whether the system flows towards either  $\mathcal{I}_1$ , or  $\mathcal{I}_2$ , or to the TKM FP, depends on the relative values of the boundary couplings at the reference scale. Based on the perturbative results we therefore infer the phase diagram of Fig.2, where we sketch the RG flow of the running coupling and highlight the various FPs that emerge from a minimal assumption on the topology of the phase diagram itself.

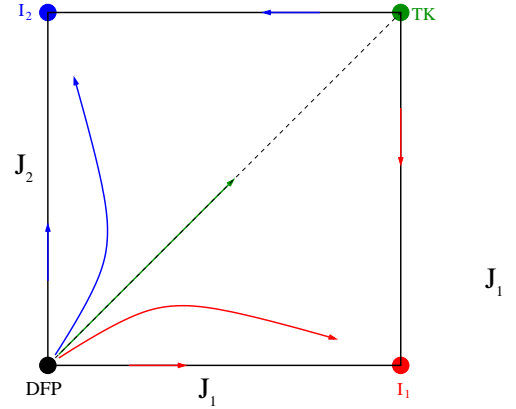


FIG. 2. Sketch of the RG trajectories and of the phase diagram of the junction in the  $J_1$ - $J_2$  plane. There are four FPs: the disconnected FP, drawn as a full black dot, at  $J_1 = J_2 = 0$ , which is fully unstable against the Kondo boundary interaction, the TK FP, drawn as a green full dot, which is reached along the RG trajectories at  $J_1 = J_2$ , but is unstable against any asymmetry between couplings  $J_1$  and  $J_2$ , the two Ising-like FPs  $\mathcal{I}_1$  and  $\mathcal{I}_2$ , respectively drawn as a full blue and red dot, which are stable and are reached along the RG flow from whatever point in parameter space with  $J_1 > J_2$ , or  $J_1 < J_2$ , respectively.

The phase diagram we draw in Fig.2 implies that, while both  $\mathcal{I}_1$  and  $\mathcal{I}_2$  are attractive FPs, there has to be a line, in parameter space, separating the RG trajectories pointing to either one of them. Apparently, the most natural choice is identifying the line with the diagonal  $J_1 = J_2$ . As we discuss in the following, this implies that the whole line, including the strongly coupled TK FP, must be unstable against any nonzero  $J_1 - J_2$ .

To study the stability of the various FPs, we first derive all possible boundary operators allowed at a specific FP from pertinent lattice model Hamiltonians (corresponding to the various putative FPs) and, then, we employ the delayed evaluation of boundary conditions (DEBC) method, originally introduced in the context of junctions of quantum wires in Ref.[26]. To illustrate how our method works, let us begin with the DFP. Formally, the disconnected junction is described by imposing open



boundary conditions at the junction site on all three the  $c_{j,\lambda}$ , that is,  $c_{0,\lambda} = c_{0,\lambda}^\dagger = 0$ ,  $\forall \lambda = 1, 2, 3$ . Retaining only low-lying modes around the Fermi points, one recovers the expansion of Eq.(A1) of Appendix A, that is

$$c_{j,\lambda} \approx e^{ik_F j} \psi_{R,\lambda}(x_j) + e^{-ik_F j} \psi_{L,\lambda}(x_j) , \quad (18)$$

with the dynamics of the chiral fermionic fields dynamics described by the Hamiltonian

$$H_0 = -i\hbar v \sum_{\lambda=1}^3 \int_0^\ell dx \{ \psi_{R,\lambda}^\dagger(x) \partial_x \psi_{R,\lambda}(x) - \psi_{L,\lambda}^\dagger(x) \partial_x \psi_{L,\lambda}(x) \} , \quad (19)$$

and  $-2J \cos(k_F) + H = 0$ ,  $x_j = aj$  (and the lattice step  $a$  set to 1 henceforth). The open boundary conditions at the junction imply

$$\begin{aligned} \psi_{R,\lambda}(0) + \psi_{L,\lambda}(0) &= 0 \\ \psi_{R,\lambda}^\dagger(0) + \psi_{L,\lambda}^\dagger(0) &= 0 . \end{aligned} \quad (20)$$

Eqs.(20) allow for “unfolding” the chiral fermionic fields, that is, for introducing a triple of chiral fields  $\{\psi_\lambda\}$ , defined for  $-\ell \leq x \leq \ell$ , such that

$$\psi_\lambda(x) = \theta(x) \psi_{R,\lambda}(x) - \theta(-x) \psi_{L,\lambda}(-x) , \quad (-\ell \leq x \leq \ell) . \quad (21)$$

Turning on a finite  $J_1$  and/or  $J_2$  and taking into account Eqs.(18,20,21), we obtain the corresponding boundary interaction Hamiltonian in the form

$$\begin{aligned} H_{K,f} = \sum_{\lambda=1}^3 \left\{ [-i\eta_\lambda \eta_{\lambda+1}] \times \right. \\ \left[ \left( \frac{\bar{J}_1 + \bar{J}_2}{2} \right) [-i(\psi_\lambda^\dagger(0) \psi_{\lambda+1}(0) - \psi_{\lambda+1}^\dagger(0) \psi_\lambda(0))] \right. \\ \left. + \left( \frac{\bar{J}_1 - \bar{J}_2}{2} \right) \sum_{\psi=1}^3 [-i(\psi_\lambda(0) \psi_{\lambda+1}(0) - \psi_{\lambda+1}^\dagger(0) \psi_\lambda^\dagger(0))] \right] \left. \right\} , \end{aligned} \quad (22)$$

with  $\bar{J}_i = 4 \sin^2(k_F) J_i$ . The operator at the right-hand side of Eq.(22) is marginally relevant, as shown by our RG analysis of Appendix B, which implies a corresponding flow away from the DFP whenever either  $J_1$ , or  $J_2$  (or both) are  $\neq 0$ . This is enough to conclude that the DFP is a repulsive FP.

We now consider either one of the equivalent, Ising-like FP, say  $\mathcal{I}_1$ . As we discuss in detail in Appendix C,  $\mathcal{I}_1$  can be described in terms of the two triples of unfolded (over the line  $-\ell \leq x \leq \ell$ ) real fermionic fields  $\xi_\lambda(x), \bar{\zeta}_\lambda(x)$ , defined in Eqs.(C16,C20). In terms of the unfolded fields, the bulk Hamiltonian and the spin and the current operators are given by

$$\begin{aligned} H_0 &= -i\hbar v \sum_{\lambda=1}^3 \int_{-\ell}^\ell dx \{ \bar{\xi}_\lambda(x) \partial_x \xi_\lambda(x) + \bar{\zeta}_\lambda(x) \partial_x \zeta_\lambda(x) \} \\ \mathcal{J}_{S,\lambda}^z(x) &= i\hbar v \sum_{a=\pm} \bar{\xi}_\lambda(ax) \bar{\zeta}_\lambda(ax) \\ \mathcal{J}_{Q,\lambda}(x) &= -i\hbar v^2 \sum_{a=\pm 1} a \{ \bar{\xi}_\lambda(ax) \partial_x \bar{\xi}_\lambda(ax) + \bar{\zeta}_\lambda(ax) \partial_x \bar{\zeta}_\lambda(ax) \} . \end{aligned} \quad (23)$$

The leading boundary interaction at the  $\mathcal{I}_1$  FP, which we derive in detail in Appendix C, takes the form

$$\begin{aligned} H_{\mathcal{I}_1} &= -\mathcal{A} [-i \prod_{\lambda=1}^3 \bar{\xi}_\lambda(0)] \mathcal{Q} \\ &+ i\mathcal{B} \sum_{\lambda=1}^3 \{ \bar{\xi}_\lambda(0) \bar{\zeta}_{\lambda+1}(0) \bar{\zeta}_{\lambda+2}(0) \} \mathcal{Q} , \end{aligned} \quad (24)$$

with  $\mathcal{A}, \mathcal{B}$  being numerical coefficients computed in Appendix C and  $\mathcal{Q}$  being a real, fermionic zero-mode operator. The operator in Eq.(C26) has dimension 3/2, that is larger than the critical dimension (1) below which a boundary operator is relevant and, therefore, we conclude that  $\mathcal{I}_1$  is a stable attractive FP of the phase diagram. The same conclusion is reached for the FP  $\mathcal{I}_2$ , once noting that it is mapped onto  $\mathcal{I}_1$  by just swapping  $\xi_\lambda(x)$  and  $\zeta_\lambda(x)$  with each other. Thus, as already remarked above, we see that the stability of both  $\mathcal{I}_1$  and  $\mathcal{I}_2$  necessarily implies the existence of a phase boundary in the  $J_1 - J_2$  parameter space. Upon our “maximally simplified” assumption, by symmetry considerations, the natural location of the phase boundary is the line  $J_1 = J_2$ , which, in Fig.2, is represented as a black, dashed line.

In between the two stable phases there is the TK FP, which we represent as a full, green dot, in Fig.2. From the weak coupling regime, the TK FP is only accessible along RG trajectories originating from the “symmetric” initial condition,  $J_1(D_0) = J_2(D_0)$ . To describe it, it is useful to bosonize the lead Dirac fields, by introducing two triple of chiral, massless Klein-Gordon fields of opposite chirality,  $\varphi_{R,\lambda}(x)$  and  $\varphi_{L,\lambda}(x)$ , such that  $\psi_{R,\lambda}(x) = \Gamma_\lambda e^{i\varphi_{R,\lambda}(x)}$ ,  $\psi_{L,\lambda}(x) = \Gamma_\lambda e^{i\varphi_{L,\lambda}(x)}$ , with  $\Gamma_\lambda$  being real-fermion Klein factors (see Appendix D for details). Within the bosonization picture the flow between the DFP and the TK FP corresponds to a flow from Neumann boundary conditions in all three the channels, that is

$$\varphi_{R,\lambda}(0) = \varphi_{L,\lambda}(0) , \quad \forall \lambda , \quad (25)$$

at the DFP, to (still) Neumann boundary conditions in the center-of-mass channel, that is,  $\Phi_R(0) = \Phi_L(0)$ , with  $\Phi_{R(L)}(x) = \frac{1}{\sqrt{3}} \sum_{\lambda=1}^2 \varphi_{R(L),\lambda}(x)$ , and Dirichlet boundary conditions in the “relative” channels,  $\chi_{R(L),1}(x) = \frac{1}{\sqrt{2}} \{ \varphi_{R(L),1}(x) - \varphi_{R(L),2}(x) \}$ , and  $\chi_{R(L),2}(x) = \frac{1}{\sqrt{6}} \{ \varphi_{R(L),1}(x) + \varphi_{R(L),2}(x) - 2\varphi_{R(L),3}(x) \}$ , that is

$$\begin{aligned} \chi_{R,1}(0) + \chi_{L,1}(0) &= 0 \\ \chi_{R,2}(0) + \chi_{L,2}(0) &= 0 . \end{aligned} \quad (26)$$

Recovering a relevant, residual boundary operator at the TK FP requires, as we show in Appendix D, that the symmetry between  $J_1$  and  $J_2$  is broken. In this case, the relevant operator is given by

$$\delta\tilde{H}_\Delta = -4\delta\bar{J} \cos \left[ \frac{\Phi_R(0) + \Phi_L(0)}{\sqrt{3}} \right], \quad (27)$$

with  $\delta\bar{J} = \bar{J}_1 - \bar{J}_2$ , whose scaling dimension is  $d_\delta J = \frac{2}{3} < 1$ .

Putting together all the above results about the behavior of the system close to the various FP, a “minimal assumption” yields the phase diagram of Fig.2. A more complex topological structure can be assumed but, given the perfect consistency between the whole diagram and our results obtained close to the FP, our minimal assumption is likely to yield the right diagram. Specifically, we see that our Y-junction of XX chains can host both the Kondo effect as realized at a junction of critical Ising chains [50], as well as a remarkable spin version of the TK effect [31]. The TK FP, here, is realized only along the symmetric line  $J_1 = J_2$  and, in a sense, it works as a separating line between the two, stable Ising-like phases.

The peculiar topological structure of the phase diagram comes along with a peculiar behavior of the spin- and of the heat-current pattern in the various phases, which we discuss in detail in the following.

#### IV. PERTURBATIVE CALCULATION OF THE SPIN- AND OF THE HEAT-CURRENT PATTERN ACROSS THE JUNCTION

In junctions of quantum wires it has been by now well established how a synoptical analysis of the charge- and of the heat-transport across the junction provides an effective mean to map out the phase diagram of the junction [31, 32]. Therefore, here we perform a similar analysis for our Y-junction of three XX spin chains, of course by substituting the charge current with the  $z$ -component of the spin current. Importantly, while the spin current is conserved in the leads, as we show below, allowing for different spin exchange strengths in the  $x$ - and in the  $y$ -direction at the junction leads to phases in which spin conservation is violated, such as the ones corresponding to the  $\mathcal{I}_1$  and the  $\mathcal{I}_2$  FPs.

In this Section, we derive the spin- and heat-current conductance within linear response theory in the applied magnetic fields and temperature biases, to leading order in  $H_{K,f}$ . We do so by employing the Keldysh Green’s function approach which is potentially amenable to extend our derivation to nonequilibrium transport [63]. We improve our perturbative result by substituting the “bare” interaction strengths with the running ones, obtained by solving Eqs.(15).

Retaining only low-energy, long-wavelength excitations around the Fermi point, we describe the DFP in terms of the field operators in Eqs.(18) and of the corresponding

unfolded fields in Eqs.(21). Accordingly, the spin- and the heat-current operators are given by

$$\begin{aligned} \mathcal{J}_{S,\lambda}^z(x) &= \hbar v \{ \psi_\lambda^\dagger(x) \psi_\lambda(x) - \psi_\lambda^\dagger(-x) \psi_\lambda(-x) \} \\ \mathcal{J}_{Q,\lambda}(x) &= \frac{i\hbar v^2}{2} \{ \psi_\lambda^\dagger(x) \partial_x \psi_\lambda(x) - [\partial_x \psi_\lambda^\dagger(x)] \psi_\lambda(x) \\ &\quad + \psi_\lambda^\dagger(-x) \partial_x \psi_\lambda(-x) - [\partial_x \psi_\lambda^\dagger(-x)] \psi_\lambda(-x) \} . \end{aligned} \quad (28)$$

Denoting with  $\mathcal{I}_{S,\lambda}(x)$  and  $\mathcal{I}_{Q,\lambda}(x)$  the average values of  $\mathcal{J}_{S,\lambda}^z(x)$  and of  $\mathcal{J}_{Q,\lambda}(x)$ , respectively, we obtain:

$$\begin{aligned} \mathcal{I}_{S,\lambda}(x) &= -\hbar v \int \frac{d\omega}{2\pi} \{ G_{(-,+)}^\lambda(x, x; \omega) - G_{(-,+)}^\lambda(-x, -x; \omega) \} \\ \mathcal{I}_{Q,\lambda}(x) &= -i\hbar v^2 \int \frac{d\omega}{2\pi} \{ \lim_{x' \rightarrow x} \partial_{x'} G_{(-,+)}^\lambda(x', x; \omega) \\ &\quad + \lim_{x' \rightarrow -x} \partial_{x'} G_{(-,+)}^\lambda(x', -x; \omega) \} , \end{aligned} \quad (29)$$

with the Keldysh-Green’s functions in the mixed (real space - frequency) representation defined as

$$G_{(\eta,\eta')}^\lambda(x, x'; \omega) = \int dt e^{i\omega t} G_{(\eta,\eta')}^\lambda(x, x'; t) , \quad (30)$$

with

$$G_{(\eta,\eta')}^\lambda(x, x'; t) = \langle \mathbf{T}_K \psi_\lambda(x, t, \eta) \psi_\lambda^\dagger(x', 0, \eta') e^{i \int_K d\tau H_{K,j}(\tau)} \rangle , \quad (31)$$

and  $\eta, \eta'$  being Keldysh indices corresponding to the two branches over the Keldysh path  $\mathcal{K}$ , over which  $\mathbf{T}_K$  is the path-ordering operator (see Appendix 4 for details). For  $J_1 = J_2 = 0$ , one gets  $G_{(\eta,\eta')}^\lambda(x, x'; \omega) = g_{(\eta,\eta')}^\lambda(x, x'; \omega)$ , with the Green-Keldysh functions in the disconnected limit listed in Eq.(A10) of Appendix A. By direct inspection one finds that the first nonzero contributions to the currents comes to second-order in the  $J_i$ . To compute it, we need the Keldysh-Green functions computed to the same order in the boundary couplings. These are given by

$$\begin{aligned} G_{(\eta,\eta')}^\lambda(x, x'; \omega) &= g_{(\eta,\eta')}^\lambda(x, x'; \omega) \\ &- \frac{(\bar{J}_1 + \bar{J}_2)^2}{4} \sum_{\eta_1, \eta_2 = \pm 1} \eta_1 \eta_2 g_{(\eta, \eta_1)}^\lambda(x, 0; \omega) g_{(\eta_2, \eta')}^\lambda(0, x'; \omega) \\ &\times \sum_{a=\pm 1} g_{(\eta_1, \eta_2)}^{\lambda+a}(0, 0; \omega) \\ &+ \frac{(-\bar{J}_1 + \bar{J}_2)^2}{2} \sum_{\eta_1, \eta_2 = \pm 1} \eta_1 \eta_2 g_{(\eta, \eta_1)}^\lambda(x, 0; \omega) g_{(\eta_2, \eta')}^\lambda(0, x'; \omega) \\ &\times \sum_{a=\pm 1} g_{(\eta_2, \eta_1)}^{\lambda+a}(0, 0; -\omega) . \end{aligned} \quad (32)$$

To recover the spin- and the heat-conductance, we compute the right-hand side of Eq.(32) by assuming that the lead  $\lambda$  is biased by an “extra” magnetic field  $\delta H_\lambda$  and by an extra temperature  $\delta T_\lambda$  (with respect to the equilibrium values  $H$  and  $T$  that are the same for all three the leads). Then, plugging the result of Eq.(32) into Eqs.(29)

for the currents and expanding to linear order in the  $\delta H_\lambda$  and in the  $\delta T_\lambda$ , we obtain

$$I_{S,\lambda}(x) = \mathcal{A}_S(T) \{ (\bar{J}_1 + \bar{J}_2)^2 [2\delta H_\lambda - \delta H_{\lambda+1} - \delta H_{\lambda-1}] + (-\bar{J}_1 + \bar{J}_2)^2 [2\delta H_\lambda + \delta H_{\lambda+1} + \delta H_{\lambda-1}] \} , \quad (33)$$

for the spin current, with

$$\mathcal{A}_S(T) = \int \frac{d\omega}{8\pi\hbar} \left[ \frac{\beta}{v^2 \cosh^2\left(\frac{\beta\omega}{2}\right)} \right] = \frac{1}{4\pi\hbar v^2} , \quad (34)$$

and  $\bar{J}_i = 4 \sin^2(k_F) J_i$ , and

$$I_{Q,\lambda}(x) = 2(\bar{J}_1^2 + \bar{J}_2^2) \mathcal{A}_Q(T) \{ -2\delta T_\lambda + \delta T_{\lambda+1} + \delta T_{\lambda-1} \} , \quad (35)$$

with

$$\mathcal{A}_{Q,\lambda}(T) = \frac{1}{4k_B T^2 v^2 \hbar^3} \int \frac{d\omega}{2\pi} \left[ \frac{\omega^2}{\cosh^2\left(\frac{\beta\omega}{2}\right)} \right] = \frac{k_B^2 T \pi^2}{6\pi \hbar^3 v^2} , \quad (36)$$

for the heat current.

At a glance to Eqs.(33) and (35) we note that, as implied by the  $\mathbb{Z}_2$  spin symmetry of the low-energy description, no off-diagonal terms appear in the conductance tensors. Also, we point out the different sign in the spin- and in the heat-current patterns determined by the boundary terms  $\propto \bar{J}_1 + \bar{J}_2$  and  $\propto \bar{J}_1 - \bar{J}_2$ , respectively. This is determined by the different nature of the physical processes induced by the corresponding boundary interaction terms in Eq.(22). Indeed, while the boundary interaction term  $\propto \bar{J}_1 + \bar{J}_2$  commutes with the total magnetization along the  $z$  direction, the term  $\propto \bar{J}_1 - \bar{J}_2$  violates the associated conservation law. Specifically, as we depict in Fig.3 **a)**, the boundary interaction term  $\propto \bar{J}_1 + \bar{J}_2$  gives rise to spin-preserving transmission or reflection of excitations. In our conventions, the magnetization current is positive when a spin up exits or a spin down enters the junction, negative when a spin up enters or a spin down exits the junction. At a finite Zeeman field  $\delta H_\lambda$  applied to lead  $\lambda$ , a nonzero transmission amplitude from lead- $\lambda$  to leads  $\lambda \pm 1$  provides a finite, positive current in the corresponding leads. At the same time, the finite transmission amplitude comes along with a reduction in the reflection coefficient back into lead- $\lambda$  (equal to unity in the disconnected junction limit), thus providing a nonzero value for the current flowing through lead- $\lambda$ . Since the current flows toward the junction, the corresponding conductance is negative in this case. At variance, in Fig.3 **b)** we show the elementary physical processes determined by the boundary interaction term  $\propto \bar{J}_1 - \bar{J}_2$ . In this case the transmission of spin waves from lead- $\lambda$  to leads  $\lambda \pm 1$  is anomalous, in the sense that it violates spin- $z$  conservation. For instance, an incoming spin up (black dot, in the figure) is transmitted as a spin down (red dot) toward either lead. This implies a sign change in the corresponding spin current (and, of course, in the conductance) that is opposite to the previous case,

in agreement with the result of Eqs.(33,35). Importantly, within lead- $\lambda$  itself the anomalous reflection results in a backscattering with opposite spin, which would be the analogous to Andreev reflection in the fermionic description. As in the previous cases, such processes determine a negative value of the current flowing through lead- $\lambda$ . The previous argument elucidates the relative signs in the various contributions to the current pattern determined by the two boundary interaction terms. Instead, the heat current is only sensitive to whether a magnon is reflected back within the same lead it comes from, or transmitted toward a different lead, regardless of its spin. Therefore, it makes no difference whether the process involves spin-conserving or spin-flip transmission/reflection.

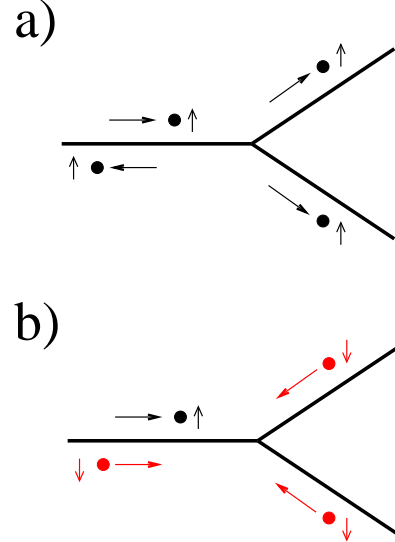


FIG. 3. Sketch of the elementary reflection/transmission processes supporting (perturbatively in the boundary couplings) spin- and heat-currents across the Y-junction, as determined respectively by the contribution to the boundary interaction term in Eq.(22) proportional to  $\bar{J}_1 + \bar{J}_2$  (**a)**), and  $\propto \bar{J}_1 - \bar{J}_2$  (**b)**). To ease reading the figure, we use full black (red) dots to denote particle (hole) like excitations within each lead. We also evidenced the spin polarization of the excitation entering/exiting the junction in each process.

Incidentally, we note that, in the symmetric case  $J_1 = J_2$ , all the (Jordan-Wigner fermion) charge (that is, physical spin) conservation violating interaction terms disappear from  $H_{K,f}$  in Eq.(22). Accordingly, the spin conductance tensor takes the only possible form allowed by the spin conservation and by the symmetry between the three channel. Specifically, we obtain

$$I_{S,\lambda}(x) = 2\bar{J}^2 \mathcal{A}_S(T) \{ 2\delta H_\lambda - \delta H_{\lambda+1} - \delta H_{\lambda-1} \} \quad (37)$$

$$I_{Q,\lambda}(x) = 4\bar{J}^2 \mathcal{A}_Q(T) \{ -2\delta T_\lambda + \delta T_{\lambda+1} + \delta T_{\lambda-1} \} ,$$

with  $\bar{J} = \bar{J}_1 = \bar{J}_2$ . In this case, as already noted in Refs.[31, 32], the Wiedemann-Franz law is recovered, as a direct consequence of the absence of the anomalous scattering processes at the junction.

Consistently to our previous RG analysis, we improve the results of Eqs.(33,35) by substituting the bare couplings with the running ones,  $\bar{J}_1(D), \bar{J}_2(D)$ , which dynamically depend on the running energy scale  $D$  (which we eventually identify with  $k_B T$ ). To determine their functional dependence on  $D$  at given values of the system parameters, one should integrate Eqs.(15). However, to qualitatively illustrate the main trend of the conductance tensors when entering the nonperturbative regime, we may employ the simplified Eqs.(B16), thus getting

$$\bar{J}_{1,2}(T) \approx \frac{\bar{J}_{1,2}(D_0)}{1 + \frac{3\bar{J}_{1,2}(D_0)}{\pi v} \ln\left(\frac{k_B T}{D_0}\right)} . \quad (38)$$

Eqs.(38) imply a logarithmic increase of both running couplings, until  $T$  reaches the Kondo temperature in whichever channel has the largest bare boundary coupling ( $\bar{J}_{1,2}(D_0)$ ). This implies that, on lowering  $T$  toward the Kondo temperature,  $I_{S,\lambda}(x) \rightarrow 4\bar{J}^2 \mathcal{A}_S(T) \delta H_\lambda$ . This is, in fact, consistent with the results that we derive in the next Section for the  $\mathcal{I}_1$  and  $\mathcal{I}_2$  FPs.

## V. SPIN AND HEAT CURRENT AT THE ISING-LIKE FIXED POINT

In Appendix C we derive in detail the field-theory description of the  $\mathcal{I}_1$  and of the  $\mathcal{I}_2$  FPs of the phase diagram of the junction. In particular, we introduce the formal description of the system at the FP in terms of a pair of triples of chiral real-fermionic field operators,  $\{\xi_\lambda(x), \bar{\zeta}_\lambda(x)\}$ , so that the FP Hamiltonian and the current density operators take the expression listed in Eqs.(23). As a result, we note that, while the FP Hamiltonian apparently takes a form similar to what we had at the DFP, the current operators are substantially different from what they are at the DFP, which we report in Eq.(28). Such a difference has important consequences for the transport properties of the system at the  $\mathcal{I}_1$  FP, as we are going to discuss next.

As we have done at the DFP, to compute the currents, we again resort to Keldysh approach, so to eventually obtain

$$\begin{aligned} I_{S,\lambda}(x) &= -\hbar v \lim_{x' \rightarrow x} \sum_{a=\pm 1} \int \frac{d\omega}{2\pi} \times \\ &\quad \{G_{(+,-)}^\lambda(ax, ay; \omega) + G_{(-,+)}^\lambda(ay, ax; \omega)\} \\ I_{Q,\lambda}(x) &= -i\hbar v^2 \lim_{x' \rightarrow x} \sum_{a=\pm 1} \partial_y \int \frac{d\omega}{2\pi} \times \\ &\quad \{G_{(+,-)}^\lambda(ax, ay; \omega) + G_{(-,+)}^\lambda(ay, ax; \omega)\} , \end{aligned} \quad (39)$$

with the  $G_{(\eta,\eta')}^\lambda(x, x'; \omega)$  being the Keldysh-Green functions of the  $\bar{\psi}_\lambda$ -field ( $= \frac{\bar{\xi}_\lambda + i\bar{\zeta}_\lambda}{\sqrt{2}}$ ) in frequency space. An important difference with respect to the DFP is that, at the  $\mathcal{I}_1$  FP, we already obtain a nonzero result for the spin current, even without considering (irrelevant)

boundary perturbations of the FP Hamiltonian. Indeed, using Eqs.(A11) for the Keldysh-Green functions, we obtain

$$I_{S,\lambda}(x) = -\frac{1}{2\pi} \int_{-D_0}^{D_0} d\omega \{f(-\omega + \delta H_\lambda) - f(\omega - \delta H_\lambda)\} . \quad (40)$$

In Eq.(40) we have restored the high-frequency cutoff  $D_0$ . To recover the correct result, we have, indeed, to perform all the calculations by keeping  $D_0$  finite and by sending  $D_0 \rightarrow \infty$  only at the end of the whole derivation. As a result, we obtain

$$I_{S,\lambda}(x) = -\frac{\hbar \delta H_\lambda}{\pi} . \quad (41)$$

At variance, for the heat current we obtain  $I_{Q,\lambda}(x) = 0$ . Remarkably, while for both the spin, and the heat, transport there is no conductance between different chains at the  $\mathcal{I}_1$  FP, from Eq.(41) we note a saturation of the intra-channel spin conductance, up to the twice the maximum value it should take in a ballistic spin conductor. In fact, such a behavior strongly resembles what happens at a junction between a p-wave superconductor in its topological phase and a spinless quantum wire [32, 64–66]. In that case, the saturation of the electric conductance is a result of the resonant (at the Fermi level) Andreev scattering amplitude due to the full hybridization between the degrees of freedom of the metallic lead and the zero-energy Majorana mode emerging at the NS interface. In our case we are dealing with a spin current and there is no NS interface. Yet, working by analogy we attribute the saturation of the spin conductance to the hybridization between the degrees of freedom of lead  $\lambda$  and the corresponding Klein factor. In this respect, we also point out how, since for each incoming particle/hole from the lead a single hole/particle is Andreev backscattered within the same lead, no net energy flow is realized across the lead itself, which motivates the result of a zero thermal current within each lead.

To move slightly away the  $\mathcal{I}_1$  (or the  $\mathcal{I}_2$ ). FP, we add to the FP Hamiltonian the leading boundary interaction term allowed by symmetry at that FP,  $H_{\mathcal{I}_1}$ , given by

$$H_{\mathcal{I}_1} = i\{\mathcal{A} \prod_{\lambda=1}^3 \bar{\xi}_\lambda(0) + \mathcal{B} \sum_{\lambda=1}^3 \bar{\xi}_\lambda(0) \bar{\zeta}_{\lambda+1}(0) \bar{\zeta}_{\lambda+2}(0)\} , \quad (42)$$

with  $\mathcal{A}$  and  $\mathcal{B}$  interaction strengths whose expressions in terms of the lattice Hamiltonian parameters we provide in Eqs.(C27).  $H_{\mathcal{I}_1}$  has scaling dimension  $\frac{3}{2}$  and is, therefore, an irrelevant perturbation. Being  $H_{\mathcal{I}_1}$  irrelevant, we expect it to provide corrections to the FP currents that go to zero as  $T \rightarrow 0$ . To compute them, we proceed as we have done at the DFP, that is, we employ Eqs.(39) to compute the  $G_{(\eta,\eta')}^\lambda(x, x'; t)$  to second-order in  $H_{\mathcal{I}_1}$ , we obtain



$$\begin{aligned}
G_{(\eta,\eta')}^\lambda(x,x';t) &= g_{(\eta,\eta')}^\lambda(x,x';t) + \delta G_{(\eta,\eta')}^\lambda(x,x';t) \\
\delta G_{(\eta,\eta')}^\lambda(x,x';t) &\approx -\frac{1}{2} \sum_{\eta_1,\eta_2} \int dt_1 dt_2 \eta_1 \eta_2 \times \quad (43) \\
\langle \mathbf{T}_K \bar{\psi}_\lambda(x,t,\eta) \bar{\psi}_\lambda^\dagger(x',0,\eta') H_{\mathcal{I}_1}(t_1,\eta_1) H_{\mathcal{I}_1}(t_2,\eta_2) \rangle .
\end{aligned}$$

Collecting together the result of Eq.(41) and what we get from Eq.(43), we eventually obtain

$$\begin{aligned}
I_{S,\lambda}(x) &= -\frac{\delta H_\lambda}{\pi} + \kappa_S T \{ \Sigma_S \delta H_\lambda + \Lambda_S [\delta H_{\lambda+1} + \delta H_{\lambda-1}] \} \\
I_{Q,\lambda}(x) &= \kappa_Q T^2 \{ \Sigma_Q \delta T_\lambda + \Lambda_Q [\delta H_{\lambda+1} + \delta H_{\lambda-1}] \} , \quad (44)
\end{aligned}$$

with  $\kappa_S$  and  $\kappa_Q$  being over-all constants (in the  $T \rightarrow 0$  limit) and  $\Sigma_S, \Lambda_S, \Sigma_Q, \Lambda_Q$  being numerical coefficients.

The above results readily allow us to identify the  $\mathcal{I}_1$  (as well as the  $\mathcal{I}_2$ , of course) FP with the  $N = 3$   $D^N$  FP of a junction of interacting quantum wires [32]. The perfect intra-channel spin conductance is due to the FP interplay between the physical processes shown in Fig.3. Indeed, while, at the level of algebraic structure, the theory underneath the  $\mathcal{I}_1$  FP shows no differences with respect to the one describing the DFP (in both case the three leads are disconnected), in fact, moving from the DFP to the  $\mathcal{I}_1$  FP corresponds to a change in the boundary conditions of the JW fermions from open to Andreev. It is, therefore, not surprising that all the conductances are zero but the intra-channel spin-conductance, whose value is actually twice as large as one would get for a perfectly, spin-conducting wire. At the same time, the Lorenz ratio at this FP is vanishing,  $\mathcal{L} = 0$ , indicating the strongest violation of the magnetic WF.

Subleading processes encoded in the “residual” boundary interaction of Eq.(C26) modify the FP result. Due to the irrelevance (in the RG sense) of all the operators contributing the right-hand side of Eq.(C26) we, however, find that all the corrections due to the residual boundary operators would disappear at low enough energy scales, leaving only the FP result discussed above.

As we discuss in the following, the symmetric coupling case  $J_1 = J_2$  determines a special flow direction in parameter space, along which the system flows towards a TK-like FP.

## VI. SPIN AND HEAT CURRENT AT THE TOPOLOGICAL KONDO FIXED POINT

In the symmetric coupling case  $J_1 = J_2$  our system flows toward the  $N = 3$  TK FP. In Appendix D, we resort to bosonization approach to reformulate the corresponding FP theoretical description of the system. Here we just summarize the main steps but discuss in detail the results. Starting from the bulk Hamiltonian expressed in terms of the unfolded fields, that is,

$$\begin{aligned}
H_0 &= -i\hbar v \sum_{\lambda=1}^3 \int_0^\ell dx \times \quad (45) \\
&\{ \psi_{R,\lambda}^\dagger(x) \partial_x \psi_{R,\lambda}(x) - \psi_{L,\lambda}^\dagger(x) \partial_x \psi_{L,\lambda}(x) \} ,
\end{aligned}$$

we bosonize the chiral fermionic fields by introducing two triples of chiral bosonic fields,  $\{\varphi_{R,\lambda}(x), \varphi_{L,\lambda}(x)\}$ , so to set

$$\begin{aligned}
\Gamma_\lambda \psi_{R,\lambda}(x) &= e^{i\sqrt{4\pi}\varphi_{R,\lambda}(x)} \\
\Gamma_\lambda \psi_{L,\lambda}(x) &= e^{i\sqrt{4\pi}\varphi_{L,\lambda}(x)} , \quad (46)
\end{aligned}$$

with the  $\Gamma_\lambda$  being additional Klein factor, required to preserve the correct (anti)commutation relations between fields living on different arms of the junction [37, 50]. The canonically conjugate nonchiral fields  $\phi_\lambda(x), \theta_\lambda(x)$  are therefore defined as

$$\begin{aligned}
\phi_\lambda(x) &= \varphi_{R,\lambda}(x) + \varphi_{L,\lambda}(x) \\
\theta_\lambda(x) &= \varphi_{R,\lambda}(x) - \varphi_{L,\lambda}(x) . \quad (47)
\end{aligned}$$

In terms of the canonical fields in Eqs.(47) we respectively obtain, for the spin- and for the heat-currents, the expressions

$$\begin{aligned}
\mathcal{J}_{S,\lambda}^z(x) &= \frac{\hbar v}{\pi} \partial_x \phi_\lambda(x) \\
\mathcal{J}_{Q,\lambda}(x) &= \frac{\hbar v^2}{\pi^2} \partial_x \phi_\lambda(x) \partial_x \theta_\lambda(x) . \quad (48)
\end{aligned}$$

Within bosonization framework, we note that, at the DFP, we get the boundary conditions  $\sqrt{4\pi}\varphi_{R,\lambda}(0) = \sqrt{4\pi}\varphi_{L,\lambda}(0) + 2\pi n_\lambda$ , with integer  $n_\lambda$ . This implies that  $\theta_\lambda(0)$  is a constant. As a result, we recover the boundary interaction in bosonic coordinates,  $H_\Delta$  as

$$H_B = -4\bar{J} \sum_{\lambda=1}^3 \cos[\sqrt{\pi}(\phi_\lambda(0) - \phi_{\lambda+1}(0))] . \quad (49)$$

To access the TK FP it is more effective to switch to the bosonic center-of-mass and relative coordinate,  $\Phi(x), \chi_1(x), \chi_2(x)$ , together with the corresponding dual fields  $\Theta(x), \omega_1(x), \omega_2(x)$ , defined by

$$\begin{bmatrix} \Phi(x) \\ \chi_1(x) \\ \chi_2(x) \end{bmatrix} = \begin{bmatrix} \frac{1}{\sqrt{3}} & \frac{1}{\sqrt{3}} & \frac{1}{\sqrt{3}} \\ \frac{1}{\sqrt{2}} & -\frac{1}{\sqrt{2}} & 0 \\ \frac{1}{\sqrt{6}} & \frac{1}{\sqrt{6}} & -\frac{2}{\sqrt{6}} \end{bmatrix} \begin{bmatrix} \phi_1(x) \\ \phi_2(x) \\ \phi_3(x) \end{bmatrix} , \quad (50)$$

and by

$$\begin{bmatrix} \Theta(x) \\ \omega_1(x) \\ \omega_2(x) \end{bmatrix} = \begin{bmatrix} \frac{1}{\sqrt{3}} & \frac{1}{\sqrt{3}} & \frac{1}{\sqrt{3}} \\ \frac{1}{\sqrt{2}} & -\frac{1}{\sqrt{2}} & 0 \\ \frac{1}{\sqrt{6}} & \frac{1}{\sqrt{6}} & -\frac{2}{\sqrt{6}} \end{bmatrix} \begin{bmatrix} \theta_1(x) \\ \theta_2(x) \\ \theta_3(x) \end{bmatrix} . \quad (51)$$

At the DFP, the open boundary conditions imply  $\partial_x \phi_\lambda(x=0) = 0, \forall \lambda = 1, 2, 3$ . Inverting Eqs.(51), we see that the right-hand side of Eq.(49) only depends on  $\chi_1(0)$  and  $\chi_2(0)$ . As we show in Appendix D, this implies that

the strongly coupled limit is recovered by pinning both  $\chi_1(x)$  and  $\chi_2(x)$  at  $x = 0$ , that is, by imposing Dirichlet boundary conditions on both fields, which correspond to Neumann boundary conditions over the corresponding dual fields. We therefore obtain that the strongly coupled FP is described by the boundary conditions

$$\partial_x \Phi(x=0) = \partial_x \omega_1(x=0) = \partial_x \omega_2(x=0) = 0. \quad (52)$$

Given Eq.(52), it is a simple exercise to compute the spin- and the heat-current pattern at the TK FP by resorting, for instance, to the splitting matrix method [31, 32, 67, 68]. As a result, one obtains that, to linear order in the transverse magnetic field and in the temperature bias, one gets

$$\begin{aligned} \mathcal{I}_{S,\lambda}(x) &= \sum_{\lambda_1=1}^3 \mathbf{G}_{\lambda,\lambda_1}^{S,\text{TK}} \delta H_{\lambda_1} \\ \mathcal{I}_{Q,\lambda}(x) &= \sum_{\lambda_1=1}^3 \mathbf{K}_{\lambda,\lambda_1}^{Q,\text{TK}} \delta T_{\lambda_1}, \end{aligned} \quad (53)$$

with

$$\mathbf{G}^{S,\text{TK}} = -\frac{\hbar}{3\pi} \begin{bmatrix} 2 & -1 & -1 \\ -1 & 2 & -1 \\ -1 & -1 & 2 \end{bmatrix}, \quad (54)$$

and

$$\mathbf{K}^{S,\text{TK}} = -\frac{2\pi k_B^2 T}{27\hbar} \begin{bmatrix} 2 & -1 & -1 \\ -1 & 2 & -1 \\ -1 & -1 & 2 \end{bmatrix}. \quad (55)$$

Taking the ratio between any matrix element of the heat- and of the spin-conductance tensor, we find a remarkable renormalization of the Lorenz ratio, compared to what predicted by the WF law, Eq.(1). Indeed, at the FP we obtain

$$\mathcal{L} = \frac{2\pi^2}{9} \left( \frac{k_B}{\hbar} \right)^2. \quad (56)$$

so that, comparing to (3), a factor  $2/3$  appears. As at the  $\mathcal{I}_1$  FP, we see that the WF law is violated at the TK FP, as well [31, 32]. However, differently from the “trivial” violation we found at the  $D^3$  ( $\mathcal{I}_1$ ) FP, here the combined effect of the boundary conditions in Eq.(52) and of the charge conservation implies that the low-temperature physics corresponds to the splitting of an injected JW fermion (that is, a spin-1/2 “spinon” excitation) into fractional spin excitations propagating into the other two wires (carrying  $2/3$  times of the incoming spin), and backscattered into the same wire (carrying  $1/3$  of the incoming spin). This evidences a remarkable onset of the spin-heat separation, that is, the spin analog of the charge-heat separation discussed in [31, 32]. By analogy with the “standard” TKM, we interpret the universal renormalization of the Lorenz ratio as a hallmark

of the hybridization between the real fermionic Klein factors emerging in the formal description of the junction. In this respect, it is the spin-conserving version of the saturation of the spin conductance that we discussed when analyzing the  $\mathcal{I}_1$  FP. Remarkably, the strict analogy between the behavior junctions of three interacting quantum wires and of quantum XX spin chains suggests the natural possibility of using the latter ones, that can be in principle realized in experimental devices with a quite good level of control on the system parameters, to analogically simulate the theoretically rich physics of quantum wires connected to real Majorana fermions, so far not yet unambiguously detected in experiments on real systems.

To conclude the discussion of the TK FP we note that, consistently with the phase diagram of Fig.2, we expect that the corresponding FP is unstable against in-isotropies in the spin exchange interactions at the junction along the  $x$  and the  $y$  direction in spin space. This means that, to keep consistent with our phase diagram, any nonzero  $J_1 - J_2$  should induce a relevant operator taking the junction from the TK to either the  $\mathcal{I}_1$ , or the  $\mathcal{I}_2$ , FP. Indeed, in Appendix D we construct the corresponding operator  $\delta \tilde{H}_\Delta$  by means of a systematic implementation of the DEBC method, eventually finding

$$\delta \tilde{H}_\Delta = -4(\bar{J}_1 - \bar{J}_2) \cos \left[ \frac{2\sqrt{\pi} \Phi(0)}{\sqrt{3}} \right]. \quad (57)$$

$\delta \tilde{H}_\Delta$  is a relevant operator, with scaling dimension  $d_\delta J = \frac{2}{3}$ : it provides the relevant perturbation that takes the system out of the TK FP and triggers the flow towards either one of the Ising-like FPs.

## VII. DISCUSSION AND CONCLUDING REMARKS

We have studied the boundary phase diagram of a Y junction of XX spin chain, in the presence of an anisotropic spin exchange interaction at the junction. The junction with purely isotropic XX interactions is known to have a nontrivial FP analogous to a four-channel Kondo model [37], robust against small perturbations of the coupling constants. In contrast, we have shown that this FP is unstable against an XY anisotropy in the spin exchange couplings. In particular, we have evidenced how, in the presence of the anisotropy, the system flows toward any of two equivalent Ising FPs [59, 62, 69]. As a consequence, the low-temperature magnetic conductance from one leg to another turns from the universal  $2\hbar/3\pi$  to zero, while the Lorenz ratio turns from the universal  $2\pi^2 k_B^2/9\hbar^2$  to zero. Avoiding this dangerous instability requires careful control of the experiment parameters and may hinder the observability of the four-channel, TK physics in junctions of quantum spin chains.

Regarding the observables, we have focused on the heat transport by spin waves only. In nanostructures, even electric insulators can carry gapless excitations, namely,

lattice deformations in the form of acoustic phonon modes and spin waves. Each of these carries energy and contributes to the thermal-, but not to the electric-, conductance. In addition, we have considered purely ballistic transport. Nevertheless, the presence of impurities turns out to be an important factor for the temperature dependence of the thermal conductivity in actual spin chain materials [70]. This qualitative picture can be further refined by the inclusion of the spin-phonon coupling [71] and of the details of the materials, a necessary step for comparing with experiments with crystalline samples [72–76]. We expect our study to be directly relevant in the context of cold-atomic circuits and simulators, prominently, of spin chains [77, 78]. Ising spin chains [79, 80], as well as XX [81] and XXZ chains [82] have indeed been realized using Rydberg atoms and their dipole interaction. Such synthetic systems allow, in principle, for measuring the spinon contribution to the thermal conductance [83]. Finally, we point out that pertinently shaped Y-junction traps are nowadays well within the reach of current technologies [56]: therefore, we hope that our predictions can be experimentally readily tested in the near future.

### ACKNOWLEDGMENTS

We thank Andrea Nava for insightful discussions. D. G. thanks the Heinrich Heine Universität - Düsseldorf for the kind hospitality during the completion of this work.

### DATA AVAILABILITY

The data that support the findings of this article are openly available at [84]

### Appendix A: The Green-Keldysh functions for the chiral fermionic fields

In this Appendix we derive the Green-Keldysh functions that we used to perform the perturbative calculation of the spin- and of the heat-conductance tensor in Section IV. (In this and in the following Appendixes, we set  $\hbar = 1$  for lightness of notation). As a necessary preliminary step, we derive the field-theoretical description of a single spin chain at a fixed temperature  $T$  with an “extra” magnetic field  $\delta H$  in the  $z$  direction. To do so, we retain only long-wavelength excitations around the Fermi points at  $\pm k_F$ , with  $-2J \cos(k_F) + H = 0$ . This implies the following expansion for the lattice fermionic fields

$$c_{j,\lambda} \approx e^{ik_F j} \psi_{R,\lambda}(x_j) + e^{-ik_F j} \psi_{L,\lambda}(x_j) , \quad (\text{A1})$$

with  $x_j = aj$  (and the lattice step  $a$  set to 1 henceforth),  $\psi_{R,\lambda}, \psi_{L,\lambda}$  chiral fermionic fields described by the Hamiltonian

$$H_{\text{FT}} = -iv \int_0^\ell dx \sum_{\lambda=1}^3 \times \{ \psi_{R,\lambda}^\dagger(x) \partial_x \psi_{R,\lambda}(x) - \psi_{L,\lambda}^\dagger(x) \partial_x \psi_{L,\lambda}(x) \} , \quad (\text{A2})$$

and the Fermi velocity  $v = J \sqrt{1 - (\frac{H}{2J})^2}$ . The open boundary conditions for the lattice fields at  $j = 0, \ell + 1$  imply

$$\begin{aligned} \psi_{R,\lambda}(0) + \psi_{L,\lambda}(0) &= 0 \\ e^{ik_F(\ell+1)} \psi_{R,\lambda}(\ell+1) + e^{-ik_F(\ell+1)} \psi_{L,\lambda}(\ell+1) &= 0 . \end{aligned} \quad (\text{A3})$$

Accordingly, for  $-\ell \leq x \leq \ell$ , we define a set of chiral, right-handed fermionic fields  $\psi_\lambda(x)$ , by setting

$$\psi_\lambda(x) = \begin{cases} \psi_{R,\lambda}(x) , & (0 \leq x \leq \ell) \\ -\psi_{L,\lambda}(-x) , & (-\ell \leq x < 0) \end{cases} , \quad (\text{A4})$$

which implies

$$e^{i\delta} \psi_\lambda(\ell) - e^{-i\delta} \psi_\lambda(-\ell) = 0 , \quad (\text{A5})$$

with  $\delta = k_F(\ell + 1)$ . As a result, the Hamiltonian in Eq.(A2) takes the form

$$H_{\text{FT}} = -iv \int_{-\ell}^\ell dx \sum_{\lambda=1}^3 \psi_\lambda^\dagger(x) \partial_x \psi_\lambda(x) . \quad (\text{A6})$$

Adding an extra magnetic field  $\delta H_\lambda$  to lead  $\lambda$  results in an additional Hamiltonian contribution  $H_{\delta H}$ , given by

$$H_{\delta H} = - \sum_{\lambda=1}^3 \delta H_\lambda \int_{-\ell}^\ell dx \psi_\lambda^\dagger(x) \psi_\lambda(x) . \quad (\text{A7})$$

In terms of the unfolded fields, the spin- and heat-current operators now become

$$\begin{aligned} \mathcal{J}_{S,\lambda}^z(x, t) &= v \sum_{a=\pm 1} a \psi_\lambda^\dagger(ax, t) \psi_\lambda(ax, t) \\ \mathcal{J}_{Q,\lambda}(x, t) &= -\frac{iv^2}{2} \sum_{a=\pm 1} \{ \psi_\lambda^\dagger(ax, t) \partial_x \psi_\lambda(ax, t) \\ &\quad - (\partial_x \psi_\lambda^\dagger(ax, t)) \psi_\lambda(ax, t) \} . \end{aligned} \quad (\text{A8})$$

Introducing, over a Keldysh path as the one displayed in Fig.4, the labels  $+$  and  $-$  to respectively refer to the upper and to the lower branch of the path itself, we define the single-fermion Green’s functions  $g_{(\eta,\eta')}(x, x'; t)$  as

$$g_{(\eta,\eta')}(x, x'; t) = \langle \mathbf{T}_K \psi(x, t, \eta) \psi^\dagger(x', 0, \eta') \rangle . \quad (\text{A9})$$

Thus, we obtain

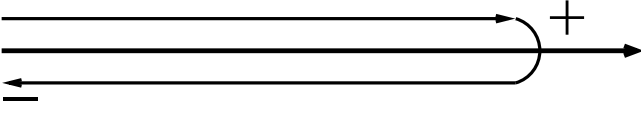


FIG. 4. Sketch of the Keldysh path with the two labels + and - attached to the corresponding branches.

$$\begin{aligned}
g_{(+,+)}(x, x'; t) &= \frac{1}{2\ell} \sum_k e^{ik(x-x')-i\epsilon_k t} \{ \theta(t) f(-\epsilon_k + \delta H) \\
&\quad - \theta(-t) f(\epsilon_k - \delta H) \} \\
g_{(+,-)}(x, x'; t) &= \frac{1}{2\ell} \sum_k e^{ik(x-x')-i\epsilon_k t} f(-\epsilon_k + \delta H) \\
g_{(-,+)}(x, x'; t) &= -\frac{1}{2\ell} \sum_k e^{ik(x-x')-i\epsilon_k t} f(\epsilon_k - \delta H) \\
g_{(-,-)}(x, x'; t) &= \frac{1}{2\ell} \sum_k e^{ik(x-x')-i\epsilon_k t} \{ \theta(-t) f(-\epsilon_k + \delta H) \\
&\quad - \theta(t) f(\epsilon_k - \delta H) \} . \tag{A10}
\end{aligned}$$

Switching to the frequency domain, according to  $g_{(\eta,\eta')}(x, x'; \omega) = \int dt e^{i\omega t} g_{(\eta,\eta')}(x, x'; t)$ , we eventually get (in the large- $\ell$  limit):

$$\begin{aligned}
g_{(+,+)}(x, x'; \omega) &= \frac{e^{\frac{i\omega}{v}(x-x')}}{2v} \left\{ \tanh \frac{\beta_\lambda(\omega - \delta H)}{2} + \epsilon(x - x') \right\} \\
g_{(+,-)}(x, x'; \omega) &= \frac{e^{\frac{i\omega}{v}(x-x')}}{v} f(-\omega + \delta H) \\
g_{(-,+)}(x, x'; \omega) &= -\frac{e^{\frac{i\omega}{v}(x-x')}}{v} f(\omega - \delta H) \\
g_{(-,-)}(x, x'; \omega) &= \frac{e^{\frac{i\omega}{v}(x-x')}}{2v} \left\{ \tanh \frac{\beta_\lambda(\omega - \delta H)}{2} - \epsilon(x - x') \right\} . \tag{A11}
\end{aligned}$$

The Green-Keldysh functions in Eqs.(A11) are what we have used in Section IV to compute the spin- and the heat-current pattern perturbatively in the Kondo boundary interaction.

## Appendix B: Mathematical derivation of the RG equations for the running Kondo parameters

In this Appendix we derive the RG equations for the running boundary couplings in the Kondo interaction Hamiltonian  $H_{K,f}$ . To do so, we write the partition function of the model as a path integral at imaginary times and systematically implement the RG procedure, thus computing the corrections to the interaction strengths arising from an infinitesimal decrease in the cutoff reference scale  $D$  [85]. In addition, to fully recover how the corresponding Kondo temperature depends on the system parameters [59], here we derive it without linearizing the dispersion relation around the Fermi points (.

Within imaginary time formalism, the Euclidean action takes the form  $\mathcal{S} = \mathcal{S}^{(0)} + \mathcal{S}_K$ , with

$$\mathcal{S}^{(0)} = \sum_{\lambda=1}^3 \mathcal{S}_\lambda^{(0)} \tag{B1}$$

$$\mathcal{S}_\lambda^{(0)} = \int_0^\beta d\tau \left\{ \sum_{j=1}^L c_{j,\lambda}^\dagger(\tau) [\partial_\tau + H] c_{j,\lambda}(\tau) - J \sum_{j=1}^L [c_{j,\lambda}^\dagger(\tau) c_{j+1,\lambda}(\tau) + c_{j+1,\lambda}^\dagger(\tau) c_{j,\lambda}(\tau)] \right\} \tag{B2}$$

$$\begin{aligned}
\mathcal{S}_K &= \left( \frac{J_1 + J_2}{2} \right) \sum_{\lambda=1}^3 \int_0^\beta d\tau \{ \mathcal{O}_1^\lambda(\tau) + [\mathcal{O}_1^\lambda(\tau)]^\dagger \} \\
&\quad + \left( \frac{J_1 - J_2}{2} \right) \sum_{\lambda=1}^3 \int_0^\beta d\tau \{ \mathcal{O}_2^\lambda(\tau) + [\mathcal{O}_2^\lambda(\tau)]^\dagger \} , \tag{B3}
\end{aligned}$$

with the operators  $\mathcal{O}_{1,2}^\lambda(\tau)$  defined as

$$\begin{aligned}
\mathcal{O}_1^\lambda(\tau) &= [-i\eta_\lambda(\tau) \eta_{\lambda+1}(\tau)] [-ic_{1,\lambda}^\dagger(\tau) c_{1,\lambda+1}(\tau)] \\
\mathcal{O}_2^\lambda(\tau) &= [-i\eta_\lambda(\tau) \eta_{\lambda+1}(\tau)] [-ic_{1,\lambda}(\tau) c_{1,\lambda+1}(\tau)] \tag{B4}
\end{aligned}$$

To derive the RG equations for  $J_1$  and  $J_2$ , we first compute  $\langle \mathcal{O}_1^\lambda(\tau) \rangle$  and  $\langle \mathcal{O}_2^\lambda(\tau) \rangle$  up to second order in the boundary interaction strengths and, then, we reabsorb the second order contributions that dynamically depend on  $D$  in a renormalization of the running couplings themselves. To do so, we need the explicit formulas for the single JW fermion and for the Klein factor correlation functions in the noninteracting theory ( $J_1 = J_2 = 0$ ). Over an  $\ell$ -site chain, these are given by

$$\begin{aligned}
\langle \mathbf{T}_\tau c_{1,\lambda}(\tau) c_{1,\lambda'}^\dagger(\tau') \rangle &= \delta_{\lambda,\lambda'} g^\lambda(\tau - \tau') = \\
&= \frac{2}{\ell + 1} \sum_k \sin^2(k) \{ [1 - f_\lambda(\epsilon_k)] e^{-\epsilon_k(\tau - \tau')} \theta(\tau - \tau') \\
&\quad - f_\lambda(\epsilon_k) e^{-\epsilon_k(\tau' - \tau)} \theta(\tau' - \tau) \} , \tag{B5}
\end{aligned}$$

with  $\mathbf{T}_\tau$  being the imaginary time ordering operator and  $f_\lambda$  being the Fermi distribution function for chain- $\lambda$ , and by

$$\langle \mathbf{T}_\tau \eta_\lambda(\tau) \eta_{\lambda'}(\tau') \rangle = \delta_{\lambda,\lambda'} \epsilon(\tau - \tau') , \tag{B6}$$

with  $\epsilon(\tau)$  being the sign function. In terms of the Green's functions in Eqs.(B5,B6) and up to second order in  $J_1$  and  $J_2$ , we obtain:



$$\begin{aligned}
\langle \mathcal{O}_1^\lambda(\tau) \rangle &= \left( \frac{J_1 + J_2}{2} \right) \frac{1}{\beta} \sum_{i\omega} g^\lambda(i\omega) g^{\lambda+1}(i\omega) \\
&\quad - \left( \frac{J_1 + J_2}{2} \right)^2 \frac{1}{\beta^3} \sum_{i\omega_1, i\omega_2} g^\lambda(i\omega_1) g^{\lambda+1}(i\omega_2) \times \\
&\quad \sum_{i\Omega} [\epsilon(i\Omega - i\omega_1) \epsilon(i\Omega - i\omega_2) \tilde{g}^{\lambda+2}(i\Omega)] \\
&\quad - \left( \frac{J_1 - J_2}{2} \right)^2 \frac{1}{\beta^3} \sum_{i\omega_1, i\omega_2} g^\lambda(i\omega_1) g^{\lambda+1}(i\omega_2) \times \\
&\quad \sum_{i\Omega} [\epsilon(i\Omega - i\omega_1) \epsilon(i\Omega - i\omega_2) \tilde{g}^{\lambda+2}(-i\Omega)] ,
\end{aligned} \tag{B7}$$

and

$$\begin{aligned}
\langle \mathcal{O}_2^\lambda(\tau) \rangle_2 &= - \left( \frac{J_1 - J_2}{2} \right) \frac{1}{\beta} \sum_{i\omega} g^\lambda(i\omega) g^{\lambda+1}(-i\omega) \\
&\quad - \frac{J_1^2 - J_2^2}{4} \frac{1}{\beta^3} \sum_{i\omega_1, i\omega_2} g^\lambda(i\omega_1) g^{\lambda+1}(-i\omega_2) \times \\
&\quad \sum_{i\Omega} [\epsilon(i\Omega - i\omega_1) \epsilon(-i\Omega + i\omega_2) \tilde{g}^{\lambda+2}(-i\Omega)] \\
&\quad - \frac{J_1^2 - J_2^2}{4} \frac{1}{\beta^3} \sum_{i\omega_1, i\omega_2} g^\lambda(i\omega_1) g^{\lambda+1}(-i\omega_2) \times \\
&\quad \sum_{i\Omega} [\epsilon(i\Omega - i\omega_1) \epsilon(-i\Omega + i\omega_2) \tilde{g}^{\lambda+2}(i\Omega)] ,
\end{aligned} \tag{B8}$$

with  $\omega_1, \omega_2$  ( $\Omega$ ) denoting fermionic (bosonic) Matsubara frequencies, and

$$\begin{aligned}
g^\lambda(i\omega) &= \int_0^\beta d\tau e^{i\omega\tau} g^\lambda(\tau) = -\frac{2}{\ell+1} \sum_k \left[ \frac{\sin^2(k)}{i\omega - \epsilon_k} \right] \\
&= \frac{i}{J} \sqrt{1 - \left( \frac{i\omega - H}{2J} \right)^2} \\
\epsilon(i\omega) &= \frac{1}{2} \int_{-\beta}^\beta d\tau e^{i\omega\tau} \epsilon(\tau) = -\frac{2}{i\omega} \\
\tilde{g}^\lambda(i\Omega) &= \frac{1}{\beta} \sum_{i\omega} g^\lambda(i\omega) \epsilon(i\Omega - i\omega) \\
&= \frac{2}{\ell+1} \sum_k \left[ \frac{\sin^2(k) \tanh\left(\frac{\beta\epsilon_k}{2}\right)}{i\Omega - \epsilon_k} \right] .
\end{aligned} \tag{B9}$$

Now, following the recipe of Ref.[59], we recover the RG equations for the running couplings  $\mathcal{J}_g = \frac{J_1+J_2}{2}$  and  $\mathcal{J}_u = \frac{J_1-J_2}{2}$  by first trading the sums over  $i\omega_2$  for integrals and by introducing a pertinent cutoff  $D$ , according to

$$\frac{1}{\beta} \sum_{i\omega_2} \rightarrow \int_{-D}^D \frac{d\omega_2}{2\pi} . \tag{B10}$$

Next, we rescale the cutoff  $D \rightarrow D - \delta D$  and renormalize the running coupling accordingly:  $\mathcal{J}_{g,u} \rightarrow \mathcal{J}_{g,u} + \delta\mathcal{J}_{g,u}(D)$ . Finally, we divide by  $\delta D$  the parameter renormalization. As a result, in the limit in which we assume that the relevant frequencies are  $\ll D$ , we obtain

$$\begin{aligned}
\frac{d\mathcal{J}_g}{dD} &= -\frac{6}{\pi JD} \varphi(D, H) \{ \mathcal{J}_g^2 + \mathcal{J}_u^2 \} \\
\frac{d\mathcal{J}_u}{dD} &= -\frac{6}{\pi JD} \varphi(D, H) 2\mathcal{J}_g \mathcal{J}_u ,
\end{aligned} \tag{B11}$$

with

$$\begin{aligned}
\varphi(D, H) &= \Re e \sqrt{1 + \left( \frac{D + iH}{2J} \right)^2} \\
&= \left\{ 1 + \frac{D^2 - H^2}{2J^2} + \left[ \frac{D^2 + H^2}{4J^2} \right]^2 \right\}^{\frac{1}{4}} \times \\
&\quad \cos \left[ \frac{1}{2} \text{atan} \left( \frac{2HD}{4J^2 + D^2 - H^2} \right) \right] .
\end{aligned} \tag{B12}$$

Eqs.(B11) decouple, once written in terms of the original running couplings  $J_{1,2}(D)$ . In particular, one gets

$$\frac{dJ_{1,2}}{dD} = -\frac{6}{\pi JD} \varphi(D, H) J_{1,2}^2 , \tag{B13}$$

which implies

$$J_{1,2}(D) = \frac{J_{1,2}(D_0)}{1 + \frac{6J_{1,2}(D_0)}{\pi J} \int_{D_0}^D \left[ \frac{\varphi(u, H)}{u} \right] du} . \tag{B14}$$

Eq.(B14) implies, for the Kondo temperatures associated to the running couplings, the expressions  $T_{k,(1,2)}$ , defined as

$$\frac{\pi J}{6J_{1,2}(D_0)} = \int_{k_B T_{k,(1,2)}}^{D_0} \left[ \frac{\varphi(u, H)}{u} \right] du . \tag{B15}$$

A numerical integration of Eqs.(B13) is straightforward and would yield, as a byproduct, the full dependence of  $T_{K,(1,2)}$  on  $H$ . However, we may find a reasonable analytic approximation by considering that the relevant contribution to the diverging RG flow of the running couplings comes from the  $D \rightarrow 0$  limit. Accordingly, for the purpose of estimating the Kondo temperature we may approximate Eqs.(B13) as

$$\frac{dJ_{1,2}}{dD} \approx - \left[ \frac{6\varphi(0, H)}{\pi JD} \right] J_{1,2}^2 , \tag{B16}$$

which yields

$$T_{K,(1,2)} \approx D_0 e^{-\frac{\pi J}{6J_{1,2}(D_0) \left[ 1 - \frac{H^2}{4J^2} \right]^{\frac{1}{2}}}} . \tag{B17}$$

Eq.(B17) implies a finite- $H$  decrease of  $T_{K,(1,2)}$  from the symmetric limit  $H = 0$  depending on  $1 - \frac{H^2}{4J^2}$ , which is consistent with the results derived in the XX limit in the lattice model studied in Ref.[59]. Starting from the RG Eqs.(B13) we recover the phase diagram discussed in the main text.

### Appendix C: Effective theory for the Ising-like fixed points

As we discuss above, an unbalance between the bare couplings  $J_1$  and  $J_2$  may trigger an RG flow towards a FP where only one of the two Kondo-like couplings in  $H_K$  turns into the strongly coupled regime. In this Appendix, we derive the effective description of the corresponding, strongly coupled FP. As we show below, the FPs shares several features with the strongly coupled fixed point of a Y junction of three critical Ising chain [39, 40, 50], yet, with the remarkable difference that, in our case, we can define a conserved spin current in the XX chains.

To achieve our purpose, we introduce real chiral fermionic fields  $\xi_{R(L),\lambda}(x)$ ,  $\zeta_{R(L),\lambda}(x)$ , that are related to  $\psi_{R(L),\lambda}(x)$  by means of the relations

$$\begin{aligned}\psi_{R(L),\lambda}(x,t) &= \frac{1}{\sqrt{2}}\{\xi_{R(L),\lambda}(x,t) + i\zeta_{R(L),\lambda}(x,t)\} \\ \psi_{R(L),\lambda}^\dagger(x,t) &= \frac{1}{\sqrt{2}}\{\xi_{R(L),\lambda}(x,t) - i\zeta_{R(L),\lambda}(x,t)\}\end{aligned}\quad (C1)$$

In terms of  $\xi_{R(L),\lambda}^\dagger$  and of  $\zeta_{R(L),\lambda}^\dagger$ , we obtain

$$\begin{aligned}H_0 &= -iv \int_{-\ell}^{\ell} dx \sum_{\lambda=1}^3 \{\xi_{R,\lambda}(x) \partial_x \xi_{R,\lambda}(x) + \zeta_{R,\lambda}(x) \partial_x \zeta_{R,\lambda}(x)\} \\ &\quad + iv \int_{-\ell}^{\ell} dx \sum_{\lambda=1}^3 \{\xi_{L,\lambda}(x) \partial_x \xi_{L,\lambda}(x) + \zeta_{L,\lambda}(x) \partial_x \zeta_{L,\lambda}(x)\}\end{aligned}$$

At the DFP the open boundary conditions on the  $\psi_\lambda$  fields at  $x=0$  in Eqs.(A3) translate into analogous conditions on the real fermionic fields, given by

$$\begin{aligned}\xi_{R,\lambda}(0) + \xi_{L,\lambda}(0) &= 0 \\ \zeta_{R,\lambda}(0) + \zeta_{L,\lambda}(0) &= 0.\end{aligned}\quad (C3)$$

Given Eqs.(C3), we unfold the chiral real fermionic fields and define two triples of real fields  $\{\xi_\lambda(x), \zeta_\lambda(x)\}$ , defined for  $-\ell \leq x \leq \ell$ , given by

$$\begin{aligned}\xi_\lambda(x) &= \theta(x)\xi_{R,\lambda}(x) - \theta(-x)\xi_{L,\lambda}(-x) \\ \zeta_\lambda(x) &= \theta(x)\zeta_{R,\lambda}(x) - \theta(-x)\zeta_{L,\lambda}(-x).\end{aligned}\quad (C4)$$

The partition function at the DFP in the  $\xi$ -sector,  $\mathcal{Z}_\xi$ , can be computed following the standard procedure of 1+1-dimensional conformal field theories (CFT) [86]. As a result, one obtains

$$\mathcal{Z}_\xi = \{q^{-\frac{1}{24}} \prod_{m=0}^{\infty} \{1 + q^{(m+\frac{1}{2})}\}\}^3, \quad (C5)$$

with  $q = \exp\left[-\frac{\beta 2\pi v}{2\ell}\right]$ . Expanding the right-hand side of Eq.(C5) around  $q=0$ , one gets, for the disconnected junction

$$\mathcal{Z}_\xi = q^{\frac{1}{16}} \{1 + 3q^{\frac{1}{2}} + 3q + 4q^{\frac{3}{2}} + \dots\}. \quad (C6)$$

From the standard CFT analysis of Eq.(C6) we conclude that the “1” corresponds to the primary field given by the identity operator, the “ $q^{\frac{1}{2}}$ ” corresponds to the triple of primary fields realized by the real fermions of scaling dimensions  $\frac{1}{2}$  [86]. The “ $3q$ ” accounts for the three, dimension-1, level-1 descendants of the identity, that is, the three currents  $\mathcal{J}_\lambda(x)$  given by

$$\mathcal{J}_\lambda(x) = -i\xi_{\lambda+1}(x)\xi_{\lambda+2}(x), \quad (C7)$$

which close the level-2,  $su(2)$  affine algebra

$$[\mathcal{J}_\lambda(x), \mathcal{J}_{\lambda'}(x')] = i\epsilon_{\lambda,\lambda',\lambda''}\delta(x-x')\mathcal{J}_{\lambda''}(x') - \frac{i}{2\pi}\delta'(x-x'), \quad (C8)$$

with  $\epsilon_{\lambda,\lambda',\lambda''}$  being the Levi-Civita symbol. A similar construction holds for the  $\zeta$ -sector of the theory, as well. As a result, on turning on  $J_1$  and  $J_2$ , we may rewrite the boundary Kondo Hamiltonian  $H_{K,f}$  as

$$\begin{aligned}H_{K,f} &= \bar{J}_1 \sum_{\lambda=1}^3 [-i\xi_\lambda(0)\xi_{\lambda+1}(0)][-i\eta_\lambda\eta_{\lambda+1}] \\ &\quad + \bar{J}_2 \sum_{\lambda=1}^3 [-i\zeta_\lambda(0)\zeta_{\lambda+1}(0)][-i\eta_\lambda\eta_{\lambda+1}].\end{aligned}\quad (C9)$$

Similarly, we may express the spin- and the heat-current operators as

$$\begin{aligned}(C2) \quad \mathcal{J}_{S,\lambda}^z(x,t) &= iv\{\xi_\lambda(x,t)\zeta_\lambda(x,t) - \xi_\lambda(-x,t)\zeta_\lambda(-x,t)\} \\ \mathcal{J}_{Q,\lambda}(x,t) &= -iv^2 \sum_{a=\pm 1} \{\xi_\lambda(ax,t)\partial_x \xi_\lambda(ax,t) \\ &\quad + \zeta_\lambda(ax,t)\partial_x \zeta_\lambda(ax,t)\}.\end{aligned}\quad (C10)$$

In the case in which  $J_2 = 0$ , the model described by  $H_\xi + H_{K,f}$ , with

$$H_\xi = -iv \sum_{\lambda=1}^3 \int_{-\ell}^{\ell} dx \xi_\lambda(x) \partial_x \xi_\lambda(x), \quad (C11)$$

corresponds to the realization of the two-channel Kondo model (2CK) originally proposed and discussed in Ref.[62]. Within such a formulation of the 2CK, it is possible to construct a simple, field-theoretical description of the system at the Kondo FP, by adapting to our specific case a trick typically employed within the CFT approach to the Kondo effect [87]. Specifically, we note that

$$H_\xi + H_{K,f} = \pi v \sum_{\lambda=1}^3 \int_{-\ell}^{\ell} dx \left\{ [\mathcal{J}_\lambda(x)]^2 + \frac{\bar{J}_1}{\pi v} \mathcal{J}_\lambda(x) \mathcal{T}_\lambda \delta(x) \right\}. \quad (C12)$$

As a result, on defining the shifted current triplet  $\mathcal{I}_\lambda(x)$  as

$$\mathcal{I}_\lambda(x) = \mathcal{J}_\lambda(x) + \frac{\bar{J}_1}{2\pi v} \mathcal{T}_\lambda \delta(x) , \quad (\text{C13})$$

we see that, for  $\frac{\bar{J}_1}{2\pi v} = 1$ , apart for an unessential constant, Eq.(C12) can be rewritten as

$$H_\xi + H_{K,f} = \pi v \sum_{\lambda=1}^3 \int_{-\ell}^{\ell} dx \{ \mathcal{I}_\lambda(x) \}^2 , \quad (\text{C14})$$

with the triple  $\mathcal{I}_\lambda(x)$  closing exactly the same affine algebra as  $\mathcal{J}_\lambda(x)$  (see Eq.(C8)). As a result, we conclude that the 2CK FP is the same as the disconnected FP, except that the local topological spin has been reabsorbed in the  $su(2)$  affine current. As there is no longer the local topological spin operator available, the leading boundary operator at the 2CK FP has to be separately constructed, as we outline in the remaining part of this Appendix, in which we employ the lattice fermion formalism to recover the (mostly relevant) leading boundary operators allowed at the  $\mathcal{I}_1$  FP.

In fact, moving from the DFP to the  $\mathcal{I}_1$  FP just corresponds to a pertinent change in the boundary conditions of the real fermionic fields at the junction. To recover it, we rewrite  $H_{K,f}$  without previously assuming any specific boundary condition on the fermionic fields as  $H_{K,f} = H_{K,f,1} + H_{K,f,2}$ , with

$$\begin{aligned} H_{K,f,1} &= -iJ_1 \sum_{\lambda=1}^3 (\bar{\xi}_{R,\lambda}(0) + \bar{\xi}_{L,\lambda}(0)) \times \\ &\quad (\bar{\xi}_{R,\lambda+1}(0) + \bar{\xi}_{L,\lambda+1}(0)) [-i\eta_\lambda \eta_{\lambda+1}] \\ H_{K,f,2} &= -iJ_2 \sum_{\lambda=1}^3 (\bar{\zeta}_{R,\lambda}(0) + \bar{\zeta}_{L,\lambda}(0)) \times \\ &\quad (\bar{\zeta}_{R,\lambda+1}(0) + \bar{\zeta}_{L,\lambda+1}(0)) [-i\eta_\lambda \eta_{\lambda+1}] , \end{aligned} \quad (\text{C15})$$

and

$$\begin{aligned} \bar{\xi}_{R,\lambda}(x) &= \cos(k_F) \xi_{R,\lambda}(x) - \sin(k_F) \zeta_{R,\lambda}(x) \\ \bar{\xi}_{L,\lambda}(x) &= \cos(k_F) \xi_{L,\lambda}(x) + \sin(k_F) \zeta_{L,\lambda}(x) \\ \bar{\zeta}_{R,\lambda}(x) &= \sin(k_F) \xi_{R,\lambda}(x) + \sin(k_F) \zeta_{R,\lambda}(x) \\ \bar{\zeta}_{L,\lambda}(x) &= -\sin(k_F) \xi_{L,\lambda}(x) + \cos(k_F) \zeta_{L,\lambda}(x) . \end{aligned} \quad (\text{C16})$$

According to Eqs.(C16), when expressing in terms of the “rotated” fields the bulk Hamiltonian, we obtain

$$\begin{aligned} H_0 &= \quad (\text{C17}) \\ -iv \sum_{\lambda=1}^3 \int_0^\ell dx \{ \bar{\xi}_{R,\lambda}(x) \partial_x \bar{\xi}_{R,\lambda}(x) + \bar{\zeta}_{R,\lambda}(x) \partial_x \bar{\zeta}_{R,\lambda}(x) \} \\ +iv \sum_{\lambda=1}^3 \int_0^\ell dx \{ \bar{\xi}_{L,\lambda}(x) \partial_x \bar{\xi}_{L,\lambda}(x) + \bar{\zeta}_{L,\lambda}(x) \partial_x \bar{\zeta}_{L,\lambda}(x) \} . \end{aligned}$$

From our previous discussion of the  $\mathcal{I}_1$  FP we have realized that it is characterized by the possibility of

fully reabsorbing the Kondo interaction in a pertinent redefinition of the  $su(2)$  affine currents. From Eqs.(C15,C16,C17) we see that the same result is recovered by imposing pertinent boundary conditions, at  $x = 0$ , over the rotated real fermionic fields, that is

$$\begin{aligned} \bar{\xi}_{R,\lambda}(0) + \bar{\xi}_{L,\lambda}(0) &= 0 \\ \bar{\zeta}_{R,\lambda}(0) + \bar{\zeta}_{L,\lambda}(0) &= 0 . \end{aligned} \quad (\text{C18})$$

The conditions in Eqs.(C18) are analogous to the ones characterizing the DFP. However, as a consequence of the nontrivial transformations in Eqs.(C16), they come along with different results for the spin- and heat-currents at the  $\mathcal{I}_1$  FP, as the corresponding operators are now expressed, in terms of the rotated fields, as

$$\begin{aligned} \mathcal{J}_{S,\lambda}^z(x) &= iv \sum_{a=\pm} \bar{\xi}_\lambda(ax) \bar{\zeta}_\lambda(ax) \\ \mathcal{J}_{Q,\lambda}(x) &= -iv^2 \sum_{a=\pm 1} a \times \\ &\quad \{ \bar{\xi}_\lambda(ax) \partial_x \bar{\xi}_\lambda(ax) + \bar{\zeta}_\lambda(ax) \partial_x \bar{\zeta}_\lambda(ax) \} \end{aligned} \quad (\text{C19})$$

with the unfolded fields defined as

$$\begin{aligned} \bar{\xi}_\lambda(x) &= \theta(x) \bar{\xi}_{R,\lambda}(x) - \theta(-x) \bar{\xi}_{L,\lambda}(-x) \\ \bar{\zeta}_\lambda(x) &= \theta(x) \bar{\zeta}_{R,\lambda}(x) - \theta(-x) \bar{\zeta}_{L,\lambda}(-x) . \end{aligned} \quad (\text{C20})$$

In the main text we discuss the consequences of the modified formulas for the current operators for the transport properties at the junction.

To conclude this Appendix, we now construct the leading boundary perturbation of the system at the  $\mathcal{I}_1$  FP,  $H_{\mathcal{I}_1}$ . To construct  $H_{\mathcal{I}_1}$ , we move back to the lattice description of the junction. Accordingly, we write the bulk Hamiltonian as:

$$H_{\text{Lat}} = -2iJ \sum_{\lambda=1}^3 \sum_{j=-\ell}^{\ell-1} \{ \bar{\xi}_{j,\lambda} \bar{\xi}_{j+1,\lambda} + \bar{\zeta}_{j,\lambda} \bar{\zeta}_{j+1,\lambda} \} , \quad (\text{C21})$$

and  $H_{K,f,1}$  as:

$$\begin{aligned} H_{K,f,1} &= J_1 \sum_{\lambda=1}^3 [-i(\bar{\xi}_{1,\lambda} + \bar{\xi}_{-1,\lambda})(\bar{\xi}_{1,\lambda+1} + \bar{\xi}_{-1,\lambda+1})] \times \\ &\quad [-i\eta_\lambda \eta_{\lambda+1}] . \end{aligned} \quad (\text{C22})$$

To minimize  $H_{K,f,1}$  in the large- $J_1$  limit, we introduce the Dirac fermionic operators

$$d_\lambda = \frac{1}{\sqrt{2}} \left\{ \frac{\bar{\xi}_{1,\lambda} + \bar{\xi}_{-1,\lambda}}{\sqrt{2}} + i\eta_\lambda \right\} , \quad (\text{C23})$$

so that we may rewrite  $H_{K,f,1}$  as

$$H_{K,f,1} = -2J_1 \left\{ \sum_{\lambda=1}^3 \left[ d_\lambda^\dagger d_\lambda - \frac{1}{2} \right] \right\}^2 + \frac{3\bar{J}_1}{2} . \quad (\text{C24})$$

From Eq.(C24) we see that the groundstate of  $H_{K,f,1}$  is twofold degenerate. Indeed, denoting with  $|n_1, n_2, n_3\rangle$

the state with occupation number of mode  $d_\lambda$  equal to  $n_\lambda$  ( $\lambda = 1, 2, 3$ ), both  $|0, 0, 0\rangle$  and  $|1, 1, 1\rangle$  have energy  $-3J_1$ . At variance, the higher energy eigenvalue  $J_1$  is sixfold degenerate, as the corresponding eigenspace is spanned by all the states with one of the  $n_\lambda$ 's equal to 0 and the other two equal to 1, or vice versa. We now build the leading boundary perturbation at the (so far) “putative” 2CK FP, in which we have set  $J_2 = 0$  and  $J_1$  very large. To do so, we connect the central triangle to the leads by singling out of the lattice bulk Hamiltonian the term containing the  $\bar{\xi}_{1,\lambda}$  and the  $\bar{\xi}_{-1,\lambda}$  operators. This is given by

$$H_t = -\frac{i\tau}{2} \sum_{\lambda=1}^3 \{\bar{\xi}_{1,\lambda}\bar{\xi}_{2,\lambda} + \bar{\xi}_{-2,\lambda}\bar{\xi}_{-1,\lambda}\} . \quad (\text{C25})$$

Eventually we set  $\tau = J$  but, for the time being, we assume that  $\tau$  is a parameter unrelated to  $J$ . Taking into account the residual boundary operators at finite  $J_2$  and  $\tau$ , going through a systematic Schrieffer-Wolff procedure involving boundary couplings and operators and resorting to the continuum fields, on implementing the DEBC method of Ref.[26], we obtain that the leading boundary perturbation is given by

$$\begin{aligned} \hat{H}_{\mathcal{I}_1} = & -\mathcal{A}[-i \prod_{\lambda=1}^3 \bar{\xi}_\lambda(0)]\mathcal{Q} \\ & + i\mathcal{B} \sum_{\lambda=1}^3 \{\bar{\xi}_\lambda(0)\bar{\xi}_{\lambda+1}(0)\bar{\xi}_{\lambda+2}(0)\}\mathcal{Q} \\ & + \mathcal{C} \sum_{\lambda=1}^3 \{\bar{\xi}_\lambda(0)\bar{\xi}_{\lambda+1}(0)\bar{\xi}_\lambda(0)\bar{\xi}_{\lambda+1}(0)\} , \quad (\text{C26}) \end{aligned}$$

with  $\mathcal{Q}$  being a real fermionic zero-mode operators connecting the degenerate minima of  $H_{K,f,1}$  [39, 50], and

$$\begin{aligned} \mathcal{A} &= \frac{3\tau^3}{16J_1^2} \\ \mathcal{B} &= \frac{\tau J_2^2}{8J_1^2} \\ \mathcal{C} &= \frac{\tau^2 J_2}{J_1^2} . \quad (\text{C27}) \end{aligned}$$

To check the stability of  $\mathcal{I}_1$ , we employ the procedure of [26, 45, 65, 88, 89], by noting how a straightforward counting of the scaling dimension of the operators entering the right-hand side of Eq.(C26) yields the values  $d_{\mathcal{A}} = d_{\mathcal{B}} = \frac{3}{2}$ ,  $d_{\mathcal{C}} = 2$ . All the scaling dimensions are larger than the critical dimension 1 and, therefore,  $\hat{H}_{\mathcal{I}_1}$  is an *irrelevant* operator and the FP  $\mathcal{I}_1$  (as well as  $\mathcal{I}_2$ ) is, therefore, stable. Yet, as we discuss in the main text, the residual interaction in Eq.(C26) is responsible for a nonzero heat current pattern in the vicinity of the  $\mathcal{I}_1$  and of the  $\mathcal{I}_2$  FPs. Retaining only the less irrelevant contributions to  $\hat{H}_{\mathcal{I}_1}$ , we eventually recover the operator  $H_{\mathcal{I}_1}$  in Eq.(24) of the main text.

## Appendix D: RG trajectory for $J_1 = J_2$

In this section we discuss the symmetric case  $J_1 = J_2 \equiv J$ . In this case, we use the Hamiltonian  $H_{\text{FL}}$  in Eq.(A2) complemented with the boundary Kondo Hamiltonian

$$\begin{aligned} H_\Delta = & \frac{J}{2} \sum_{\lambda=1}^3 \{[-i\eta_\lambda\eta_{\lambda+1}] \times \\ & [-i[(\psi_{R,\lambda}^\dagger(0) + \psi_{L,\lambda}^\dagger(0))(\psi_{R,\lambda+1}(0) + \psi_{L,\lambda+1}(0)) \\ & + (\psi_{R,\lambda}(0) + \psi_{L,\lambda}(0))(\psi_{R,\lambda+1}^\dagger(0) + \psi_{L,\lambda+1}^\dagger(0))]\} . \quad (\text{D1}) \end{aligned}$$

To achieve the (large- $J$ ) Kondo limit, we now apply chiral bosonization to Eqs.(D1). To do so, we set [90]

$$\begin{aligned} \eta_\lambda \psi_{R,\lambda}(x) &= e^{i\sqrt{4\pi}\varphi_{R,\lambda}(x)} \\ \eta_\lambda \psi_{L,\lambda}(x) &= e^{i\sqrt{4\pi}\varphi_{L,\lambda}(x)} , \quad (\text{D2}) \end{aligned}$$

with  $\varphi_{R,\lambda}, \varphi_{L,\lambda}$  respectively being chiral, right-handed and left-handed bosonic fields (defined for  $0 \leq x \leq \ell$ ). In terms of the chiral, bosonic fields, the spin- and the heat-current operators in lead- $\lambda$  are given by [31, 32]

$$\begin{aligned} \mathcal{J}_{S,\lambda}(x) &= \frac{v}{\pi} \{\partial_x \varphi_R(x) + \partial_x \varphi_L(x)\} \\ \mathcal{J}_{Q,\lambda}(x) &= \frac{v^2}{\pi^2} \{(\partial_x \varphi_{R,\lambda}(x))^2 - (\partial_x \varphi_{L,\lambda}(x))^2\} . \quad (\text{D3}) \end{aligned}$$

In order to go through the next steps, it is useful to switch to the spin-plasmon fields  $\phi_\lambda(x)$ , together with their dual fields,  $\theta_\lambda(x)$ . These are related to the chiral fields in Eqs.(D2) via the relations

$$\begin{aligned} \phi_\lambda(x) &= \varphi_{R,\lambda}(x) + \varphi_{L,\lambda}(x) \\ \theta_\lambda(x) &= \varphi_{R,\lambda}(x) - \varphi_{L,\lambda}(x) . \quad (\text{D4}) \end{aligned}$$

The open boundary conditions translate into the relations  $\varphi_{R,\lambda}(0) = \varphi_{L,\lambda}(0)$  between opposite chirality fields. These imply the boundary conditions  $\theta_\lambda(0) = 0$ , for  $\lambda = 1, 2, 3$ , so that the boundary interaction reduces to

$$\hat{H}_\Delta = -4\bar{J} \sum_{\lambda=1}^3 \cos[\sqrt{\pi}(\phi_\lambda(0) - \phi_{\lambda+1}(0))] . \quad (\text{D5})$$

The boundary Hamiltonian in Eq.(D5) corresponds to the  $SO(3)$  TKM [53, 57, 61], with Luttinger parameter  $g = 1$ . In this case,  $H_\Delta$  is marginally relevant [52, 57, 88, 89, 91, 92], and drives the system towards a large- $\bar{J}$  Kondo FP [53, 57, 61]. Importantly,  $H_\Delta$  remains *purely bosonic*. At the DFP the boundary conditions on the fermionic fields,  $\psi_{R,\lambda}(0) + \psi_{L,\lambda}(0) = 0$ , simply translate into Neumann-like boundary conditions for the bosonic fields  $\phi_\lambda(x)$ , that is,  $\partial_x \phi_\lambda(0) = 0$ ,  $\forall \lambda$ . Now, as it is customary in analyzing junctions of quantum wires within bosonization framework [26], we switch to the center-of-mass and to the relative chiral fields,  $\Phi(x), \chi_{1,2}(x)$  (together with their dual ones), defined by



$$\begin{bmatrix} \Phi(x) \\ \chi_1(x) \\ \chi_2(x) \end{bmatrix} = \begin{bmatrix} \frac{1}{\sqrt{3}} & \frac{1}{\sqrt{3}} & \frac{1}{\sqrt{3}} \\ \frac{1}{\sqrt{2}} & -\frac{1}{\sqrt{2}} & 0 \\ \frac{1}{\sqrt{6}} & \frac{1}{\sqrt{6}} & -\frac{2}{\sqrt{6}} \end{bmatrix} \begin{bmatrix} \phi_1(x) \\ \phi_2(x) \\ \phi_3(x) \end{bmatrix}, \quad (\text{D6})$$

and by

$$\begin{bmatrix} \Theta(x) \\ \omega_1(x) \\ \omega_2(x) \end{bmatrix} = \begin{bmatrix} \frac{1}{\sqrt{3}} & \frac{1}{\sqrt{3}} & \frac{1}{\sqrt{3}} \\ \frac{1}{\sqrt{2}} & -\frac{1}{\sqrt{2}} & 0 \\ \frac{1}{\sqrt{6}} & \frac{1}{\sqrt{6}} & -\frac{2}{\sqrt{6}} \end{bmatrix} \begin{bmatrix} \theta_1(x) \\ \theta_2(x) \\ \theta_3(x) \end{bmatrix}. \quad (\text{D7})$$

In terms of the relative fields, we obtain [31, 57]

$$\tilde{H}_\Delta = 4\bar{J} \sum_{a=1}^3 \cos[\sqrt{2\pi} \hat{k}_a \cdot \vec{\chi}(0)] , \quad (\text{D8})$$

with  $\hat{k}_a = \left[ \cos\left(\frac{4\pi(a-1)}{3}\right), \sin\left(\frac{4\pi(a-1)}{3}\right) \right]$ , and  $\vec{\chi}(0) = [\chi_1(0), \chi_2(0)]$ . The emergence of a boundary Hamiltonian such as  $\tilde{H}_\Delta$  in Eq.(D8) characterizes a number of different physical contexts, such as, for instance, the theory of the quantum Brownian motion on a triangular lattice [45, 93], or a junction of three Bose liquids [94], or of three Josephson chains [49, 95]. At the DFP, the Neumann boundary conditions over the  $\phi_\lambda$  fields translate into Neumann boundary conditions for the three fields  $\Phi(x), \chi_{1,2}(x)$ , at  $x = 0$ . At variance, the FP that describes the system in the strongly coupled limit ( $J \rightarrow \infty$ ) is recovered by minimizing the corresponding boundary interaction at the right-hand side of Eq.(D8), that is, by requiring that

$$\sqrt{2\pi} \hat{k} \cdot \vec{\chi}(0) = 2\pi n_a, \quad n_a \in \mathcal{Z}, \quad (\text{D9})$$

for all  $a = 1, 2, 3$  (note that this naturally implies  $n_1 + n_2 + n_3 = 0$ ). As a result, we obtain that the Kondo FP is simply characterized by Dirichlet (rather than Neumann) boundary conditions at  $x = 0$  for the relative fields  $\chi_{1,2}(x)$ , while the center-of-mass field  $\Phi(x)$ , being decoupled from the boundary interaction, still obeys Neumann boundary conditions.

Clearly, all the discussion above applies in the case in which  $J_1 = J_2$  strictly. Consistently with the main phase diagram of our system, we expect that the TK FP is no longer stable, as soon as  $J_1 \neq J_2$ . To verify this point, let us set  $\delta\bar{J} = \bar{J}_1 - \bar{J}_2$  and let us consider the “residual” boundary Hamiltonian  $\delta H_\Delta$  emerging at  $\delta J \neq 0$ . We obtain

$$\begin{aligned} \delta H_\Delta = \delta\bar{J} \sum_{\lambda=1}^3 \{ & [-i\eta_\lambda \eta_{\lambda+1}] \times \\ & [-i[(\psi_{R,\lambda}(0) + \psi_{L,\lambda}(0))(\psi_{R,\lambda+1}(0) + \psi_{L,\lambda+1}(0)) \\ & + (\psi_{R,\lambda}^\dagger(0) + \psi_{L,\lambda}^\dagger(0))(\psi_{R,\lambda+1}^\dagger(0) + \psi_{L,\lambda+1}^\dagger(0))] \}. \end{aligned} \quad (\text{D10})$$

Bosonizing the operator at the right-hand side of Eq.(D10), we obtain

$$\delta\tilde{H}_\Delta = -4\delta\bar{J} \sum_{\lambda=1}^3 \cos[\sqrt{\pi}(\phi_\lambda(0) + \phi_{\lambda+1}(0))] , \quad (\text{D11})$$

At the TK FP, taking into account the Dirichlet boundary conditions determined by the pinning of  $\chi_{1,2}(0)$ , the only field effectively entering the right-hand side of Eq.(D11) is the center of mass field  $\Phi(x)$ . That being stated, we find that the operator at the right-hand side of Eq.(D11) becomes (57)

- 
- [1] G. Gallavotti, *The Fermi-Pasta-Ulam problem: a status report*, Vol. 728 (Springer, 2007).
- [2] F. Barra, The thermodynamic cost of driving quantum systems by their boundaries, *Scientific Reports* **5**, 10.1038/srep14873 (2015).
- [3] M. Campisi and R. Fazio, Dissipation, correlation and lags in heat engines, *Journal of Physics A: Mathematical and Theoretical* **49**, 345002 (2016).
- [4] L. Arrachea, Energy dynamics, heat production and heat-work conversion with qubits: toward the development of quantum machines, *Reports on Progress in Physics* **86**, 036501 (2023).
- [5] O. Narayan and S. Ramaswamy, Anomalous heat conduction in one-dimensional momentum-conserving systems, *Phys. Rev. Lett.* **89**, 200601 (2002).
- [6] X. Zotos, F. Naef, and P. Prelovsek, Transport and conservation laws, *Phys. Rev. B* **55**, 11029 (1997).
- [7] E. Shimshoni, N. Andrei, and A. Rosch, Thermal conductivity of spin- 1/2 chains, *Physical Review B* **68**, 104401 (2003).
- [8] T. Prosen, Open  $xxz$  spin chain: Nonequilibrium steady state and a strict bound on ballistic transport, *Phys. Rev. Lett.* **106**, 217206 (2011).
- [9] M. Bockrath, D. H. Cobden, J. Lu, A. G. Rinzler, R. E. Smalley, L. Balents, and P. L. McEuen, Luttinger-liquid behaviour in carbon nanotubes, *Nature* **397**, 598–601 (1999).
- [10] C. Blumenstein, J. Schäfer, S. Mietke, S. Meyer, A. Dollinger, M. Lochner, X. Cui, L. Patthey, R. Matzdorf, and R. Claessen, Atomically controlled quantum chains hosting a Tomonaga–Luttinger liquid, *Nature Physics* **7**, 776–780 (2011).
- [11] B. J. van Wees, H. van Houten, C. W. J. Beenakker, J. G. Williamson, L. P. Kouwenhoven, D. van der Marel, and C. T. Foxon, Quantized conductance of point contacts in a two-dimensional electron gas, *Phys. Rev. Lett.* **60**, 848 (1988).
- [12] A. De Martino, K. Dorn, F. Bucchieri, and R. Egger, Phonon-induced magnetoresistivity of Weyl semimetal nanowires, *Phys. Rev. B* **104**, 155425 (2021).
- [13] K. Wakabayashi, Y. Takane, M. Yamamoto, and M. Sigrist, Electronic transport properties of graphene nanoribbons, *New Journal of Physics* **11**, 095016 (2009).
- [14] K.-I. Uchida, S. Takahashi, K. Harii, J. Ieda, W. Koshibae, K. Ando, S. Maekawa, and E. Saitoh, Observation of the spin Seebeck effect, *nature* **455**, 778–781 (2008).
- [15] G. E. Bauer, E. Saitoh, and B. J. Van Wees, Spin

- caloritronics, *Nature materials* **11**, 391–399 (2012).
- [16] T. An, V. I. Vasyuchka, K. Uchida, A. V. Chumak, K. Yamaguchi, K. Harii, J. Ohe, M. B. Jungfleisch, Y. Kajiwara, H. Adachi, B. Hillebrands, S. Maekawa, and E. Saitoh, Unidirectional spin-wave heat conveyer, *Nature Materials* **12**, 549–553 (2013).
- [17] J. Chen, H. Yu, and G. Gubbiotti, Unidirectional spin-wave propagation and devices, *Journal of Physics D: Applied Physics* **55**, 123001 (2021).
- [18] J. Zou, S. Bosco, E. Thingstad, J. Klinovaja, and D. Loss, Dissipative spin-wave diode and nonreciprocal magnonic amplifier, *Phys. Rev. Lett.* **132**, 036701 (2024).
- [19] K.-i. Uchida and R. Iguchi, Spintronic thermal management, *Journal of the Physical Society of Japan* **90**, 122001 (2021).
- [20] T. K. Konar, S. Ghosh, A. K. Pal, and A. Sen(De), Designing robust quantum refrigerators in disordered spin models, *Phys. Rev. A* **105**, 022214 (2022).
- [21] A. A. Zvyagin and V. V. Slavin, Giant caloric effects in spin-chain materials, *Phys. Rev. B* **109**, 214438 (2024).
- [22] J.-W. Zhang, J.-Q. Zhang, G.-Y. Ding, J.-C. Li, J.-T. Bu, B. Wang, L.-L. Yan, S.-L. Su, L. Chen, F. Nori, S. K. Özdemir, F. Zhou, H. Jing, and M. Feng, Dynamical control of quantum heat engines using exceptional points, *Nature Communications* **13**, 10.1038/s41467-022-33667-1 (2022).
- [23] J.-T. Bu, J.-Q. Zhang, G.-Y. Ding, J.-C. Li, J.-W. Zhang, B. Wang, W.-Q. Ding, W.-F. Yuan, L. Chen, Q. Zhong, et al., Chiral quantum heating and cooling with an optically controlled ion, *Light: Science & Applications* **13**, 143 (2024).
- [24] N. Loft, O. Marchukov, D. Petrosyan, and N. Zinner, Tunable self-assembled spin chains of strongly interacting cold atoms for demonstration of reliable quantum state transfer, *New Journal of Physics* **18**, 045011 (2016).
- [25] O. V. Marchukov, A. G. Volosniev, M. Valiente, D. Petrosyan, and N. Zinner, Quantum spin transistor with a Heisenberg spin chain, *Nature communications* **7**, 13070 (2016).
- [26] M. Oshikawa, C. Chamon, and I. Affleck, Junctions of three quantum wires, *Journal of Statistical Mechanics: Theory and Experiment* **2006**, P02008 (2006).
- [27] M. Horvat, T. Prosen, G. Benenti, and G. Casati, Railway switch transport model, *Phys. Rev. E* **86**, 052102 (2012).
- [28] F. Barra and P. Gaspard, Transport and dynamics on open quantum graphs, *Phys. Rev. E* **65**, 016205 (2001).
- [29] B. Bellazzini, M. Burrello, M. Mintchev, and P. Sorba, Quantum field theory on star graphs (2008), arXiv:0801.2852 [hep-th].
- [30] B. Bellazzini and M. Mintchev, Quantum fields on star graphs, *J. Phys. A Math. Theor.* **39**, 11101 (2006).
- [31] F. Bucchieri, A. Nava, R. Egger, P. Sodano, and D. Giuliano, Violation of the Wiedemann-Franz law in the topological Kondo model, *Phys. Rev. B* **105**, L081403 (2022).
- [32] D. Giuliano, A. Nava, R. Egger, P. Sodano, and F. Bucchieri, Multiparticle scattering and breakdown of the Wiedemann-Franz law at a junction of  $n$  interacting quantum wires, *Phys. Rev. B* **105**, 035419 (2022).
- [33] M. Mintchev, L. Santoni, and P. Sorba, Energy transmutation in nonequilibrium quantum systems, *Journal of Physics A: Mathematical and Theoretical* **48**, 055003 (2015).
- [34] M. Mintchev, Non-equilibrium steady states of quantum systems on star graphs, *Journal of Physics A: Mathematical and Theoretical* **44**, 415201 (2011).
- [35] F. Bucchieri, R. Egger, R. G. Pereira, and F. B. Ramos, Quantum spin circulator in Y junctions of Heisenberg chains, *Phys. Rev. B* **97**, 220402 (2018).
- [36] F. Bucchieri, R. Egger, R. G. Pereira, and F. B. Ramos, Chiral Y junction of quantum spin chains, *Nuclear Physics B* **941**, 794 (2019).
- [37] N. Crampé and A. Trombettoni, Quantum spins on star graphs and the Kondo model, *Nuclear Physics B* **871**, 526 (2013).
- [38] A. M. Tsvelik and W.-G. Yin, Possible realization of a multichannel Kondo model in a system of magnetic chains, *Phys. Rev. B* **88**, 144401 (2013).
- [39] D. Giuliano and P. Sodano, Realization of a two-channel Kondo model with Josephson junction networks, *Europhysics Letters* **103**, 57006 (2013).
- [40] D. Giuliano, A. Nava, and P. Sodano, Tunable Kondo screening length at a y-junction of three inhomogeneous spin chains, *Nuclear Physics B* **960**, 115192 (2020).
- [41] N. Laflorencie, E. S. Sørensen, and I. Affleck, The Kondo effect in spin chains, *Journal of Statistical Mechanics: Theory and Experiment* **2008**, P02007 (2008).
- [42] J. Gaines, G. Li, and J. Väyrynen, Spin-chain multichannel Kondo model via image impurity boundary condition (2025), arXiv:2506.02399 [cond-mat.str-el].
- [43] K. Nakata, P. Simon, and D. Loss, Wiedemann-Franz law for magnon transport, *Phys. Rev. B* **92**, 134425 (2015).
- [44] K. Nakata, P. Simon, and D. Loss, Spin currents and magnon dynamics in insulating magnets, *Journal of Physics D: Applied Physics* **50**, 114004 (2017).
- [45] C. Chamon, M. Oshikawa, and I. Affleck, Junctions of three quantum wires and the dissipative Hofstadter model, *Phys. Rev. Lett.* **91**, 206403 (2003).
- [46] C.-Y. Hou and C. Chamon, Junctions of three quantum wires for spin- $\frac{1}{2}$  electrons, *Phys. Rev. B* **77**, 155422 (2008).
- [47] A. Cirillo, M. Mancini, D. Giuliano, and P. Sodano, Enhanced coherence of a quantum doublet coupled to Tomonaga-Luttinger liquid leads, *Nuclear Physics B* **852**, 235 (2011).
- [48] D. Giuliano and P. Sodano, Pairing of Cooper pairs in a Josephson junction network containing an impurity, *Europhysics Letters* **88**, 17012 (2009).
- [49] D. Giuliano and P. Sodano, Competing boundary interactions in a Josephson junction network with an impurity, *Nuclear Physics B* **837**, 153 (2010).
- [50] A. M. Tsvelik, Majorana fermion realization of a two-channel Kondo effect in a junction of three quantum Ising chains, *Phys. Rev. Lett.* **110**, 147202 (2013).
- [51] A. M. Tsvelik, Topological Kondo effect in star junctions of Ising magnetic chains: exact solution, *New Journal of Physics* **16**, 033003 (2014).
- [52] A. Altland and R. Egger, Multiterminal Coulomb-Majorana junction, *Phys. Rev. Lett.* **110**, 196401 (2013).
- [53] A. Altland, B. Béri, R. Egger, and A. M. Tsvelik, Multichannel Kondo impurity dynamics in a Majorana device, *Phys. Rev. Lett.* **113**, 076401 (2014).
- [54] D. Giuliano, L. Lepori, and A. Nava, Tunable spin/charge Kondo effect at a double superconducting island connected to two spinless quantum wires, *Phys. Rev. B* **101**, 195140 (2020).
- [55] D. Guerzi and A. Nava, Probing Majorana zero modes by measuring transport through an interacting magnetic im-

- purity, *Physica E: Low-dimensional Systems and Nanostructures* **134**, 114895 (2021).
- [56] F. Bucchieri, G. D. Bruce, A. Trombettoni, D. Cassettari, H. Babujian, V. E. Korepin, and P. Sodano, Holographic optical traps for atom-based topological Kondo devices, *New Journal of Physics* **18**, 075012 (2016).
  - [57] B. Béri and N. R. Cooper, Topological Kondo effect with Majorana fermions, *Phys. Rev. Lett.* **109**, 156803 (2012).
  - [58] A. Berkowitz and K. Takano, Exchange anisotropy — a review, *Journal of Magnetism and Magnetic Materials* **200**, 552 (1999).
  - [59] D. Giuliano, P. Sodano, A. Tagliacozzo, and A. Trombettoni, From four- to two-channel Kondo effect in junctions of xy spin chains, *Nuclear Physics B* **909**, 135 (2016).
  - [60] D. Giuliano, G. Campagnano, and A. Tagliacozzo, Junction of three off-critical quantum Ising chains and two-channel Kondo effect in a superconductor, *The European Physical Journal B* **89**, 251 (2016).
  - [61] F. Bucchieri, H. Babujian, V. E. Korepin, P. Sodano, and A. Trombettoni, Thermodynamics of the topological Kondo model, *Nuclear Physics B* **896**, 52 (2015).
  - [62] P. Coleman, L. B. Ioffe, and A. M. Tsvelik, Simple formulation of the two-channel Kondo model, *Phys. Rev. B* **52**, 6611 (1995).
  - [63] M. M. Wauters, C.-M. Chung, L. Maffi, and M. Burrello, Topological Kondo model out of equilibrium, *Phys. Rev. B* **108**, L220302 (2023).
  - [64] L. Fidkowski, J. Alicea, N. H. Lindner, R. M. Lutchyn, and M. P. A. Fisher, Universal transport signatures of Majorana fermions in superconductor-Luttinger liquid junctions, *Phys. Rev. B* **85**, 245121 (2012).
  - [65] I. Affleck and D. Giuliano, Topological superconductor-Luttinger liquid junctions, *Journal of Statistical Mechanics: Theory and Experiment* **2013**, P06011 (2013).
  - [66] I. Affleck and D. Giuliano, Screening clouds and Majorana fermions, *Journal of Statistical Physics* **157**, 666 (2014).
  - [67] E. Eriksson, A. Nava, C. Mora, and R. Egger, Tunneling spectroscopy of Majorana-Kondo devices, *Phys. Rev. B* **90**, 245417 (2014).
  - [68] D. Giuliano and A. Nava, Dual fermionic variables and renormalization group approach to junctions of strongly interacting quantum wires, *Phys. Rev. B* **92**, 125138 (2015).
  - [69] A. Zazunov, F. Bucchieri, P. Sodano, and R. Egger,  $6\pi$  Josephson effect in Majorana box devices, *Phys. Rev. Lett.* **118**, 057001 (2017).
  - [70] A. V. Rozhkov and A. L. Chernyshev, Thermal conductivity of quasi-one-dimensional antiferromagnetic spin-chain materials, *Phys. Rev. Lett.* **94**, 087201 (2005).
  - [71] K. Louis, P. Prelovšek, and X. Zotos, Thermal conductivity of one-dimensional spin-1/2 systems coupled to phonons, *Phys. Rev. B* **74**, 235118 (2006).
  - [72] A. L. Chernyshev and A. V. Rozhkov, Heat transport in spin chains with weak spin-phonon coupling, *Phys. Rev. Lett.* **116**, 017204 (2016).
  - [73] A. V. Sologubenko, E. Felder, K. Giannò, H. R. Ott, A. Vietkine, and A. Revcolevschi, Thermal conductivity and specific heat of the linear chain cuprate  $\text{Sr}_2\text{CuO}_3$  : evidence for thermal transport via spinons, *Phys. Rev. B* **62**, R6108 (2000).
  - [74] A. V. Sologubenko, K. Giannò, H. R. Ott, U. Ammerahl, and A. Revcolevschi, Thermal conductivity of the hole-doped spin ladder system  $\text{Sr}_{14-x}\text{Ca}_x\text{Cu}_{24}\text{O}_{41}$ , *Phys. Rev. Lett.* **84**, 2714 (2000).
  - [75] A. V. Sologubenko, K. Giannò, H. R. Ott, A. Vietkine, and A. Revcolevschi, Heat transport by lattice and spin excitations in the spin-chain compounds  $\text{SrCuO}_2$  and  $\text{Sr}_2\text{CuO}_3$ , *Phys. Rev. B* **64**, 054412 (2001).
  - [76] B. Y. Pan, Y. Xu, J. M. Ni, S. Y. Zhou, X. C. Hong, X. Qiu, and S. Y. Li, Unambiguous experimental verification of linear-in-temperature spinon thermal conductivity in an antiferromagnetic heisenberg chain, *Phys. Rev. Lett.* **129**, 167201 (2022).
  - [77] R. Toskovic, R. Van Den Berg, A. Spinelli, I. Eliens, B. Van Den Toorn, B. Bryant, J.-S. Caux, and A. Otte, Atomic spin-chain realization of a model for quantum criticality, *Nature Physics* **12**, 656 (2016).
  - [78] P. N. Jepsen, J. Amato-Grill, I. Dimitrova, W. W. Ho, E. Demler, and W. Ketterle, Spin transport in a tunable Heisenberg model realized with ultracold atoms, *Nature* **588**, 403 (2020).
  - [79] P. Schauss, Quantum simulation of transverse Ising models with Rydberg atoms, *Quantum Science and Technology* **3**, 023001 (2018).
  - [80] A. Browaeys and T. Lahaye, Many-body physics with individually controlled Rydberg atoms, *Nature Physics* **16**, 132 (2020).
  - [81] S. Geier, N. Thaicharoen, C. Hainaut, T. Franz, A. Salzinger, A. Tebben, D. Grimshandl, G. Zürn, and M. Weidemüller, Floquet Hamiltonian engineering of an isolated many-body spin system, *Science* **374**, 1149 (2021).
  - [82] T. Franz, S. Geier, C. Hainaut, A. Braemer, N. Thaicharoen, M. Hornung, E. Braun, M. Gärttner, G. Zürn, and M. Weidemüller, Observation of anisotropy-independent magnetization dynamics in spatially disordered heisenberg spin systems, *Phys. Rev. Res.* **6**, 033131 (2024).
  - [83] D. Hirobe, M. Sato, T. Kawamata, Y. Shiomi, K.-i. Uchida, R. Iguchi, Y. Koike, S. Maekawa, and E. Saitoh, One-dimensional spinon spin currents, *Nature Physics* **13**, 30 (2017).
  - [84] D. Giuliano and F. Bucchieri, Dataset (analytical calculations) for the paper “Spin and thermal current scaling at a Y-junction of XX spin chains”, Zenodo 10.5281/zenodo.16863701.
  - [85] A. C. Hewson, *The Kondo problem, in The Kondo Problem to Heavy Fermions*, Cambridge Studies in Magnetism (Cambridge University Press, 1993).
  - [86] P. Di Francesco, P. Mathieu, and D. Senechal, *Conformal Field Theory*, Graduate Texts in Contemporary Physics (Springer-Verlag, New York, 1997).
  - [87] I. Affleck, Conformal field theory approach to the Kondo effect, *Acta Phys. Polon. B* **26**, 1869 (1995).
  - [88] D. Giuliano and I. Affleck, Real fermion modes, impurity entropy, and nontrivial fixed points in the phase diagram of junctions of interacting quantum wires and topological superconductors, *Nuclear Physics B* **944**, 114645 (2019).
  - [89] C. L. Kane, D. Giuliano, and I. Affleck, Equivalent critical behavior of a helical point contact and a two-channel Luttinger liquid-topological superconductor junction, *Phys. Rev. Res.* **2**, 023243 (2020).
  - [90] K. Michaeli, L. A. Landau, E. Sela, and L. Fu, Electron teleportation and statistical transmutation in multiterminal Majorana islands, *Phys. Rev. B* **96**, 205403 (2017).
  - [91] J. Cardy, *Scaling and Renormalization in Statistical Physics*,

- Cambridge Lecture Notes in Physics (Cambridge University Press, 1996).
- [92] D. Giuliano, D. Rossini, and A. Trombettoni, From Kondo effect to weak-link regime in quantum spin- $\frac{1}{2}$  spin chains, *Phys. Rev. B* **98**, 235164 (2018).
  - [93] H. Yi and C. L. Kane, Quantum brownian motion in a periodic potential and the multichannel Kondo problem, *Phys. Rev. B* **57**, R5579 (1998).
  - [94] A. Tokuno, M. Oshikawa, and E. Demler, Dynamics of one-dimensional bose liquids: Andreev-like reflection at  $y$  junctions and the absence of the Aharonov-Bohm effect, *Phys. Rev. Lett.* **100**, 140402 (2008).
  - [95] D. Giuliano and P. Sodano, Frustration of decoherence in y-shaped superconducting Josephson networks, *New Journal of Physics* **10**, 093023 (2008).